

Toward Soft Skin-Like Wearable and Implantable Energy Devices

Shu Gong and Wenlong Cheng*

The development of ultra-compliant power sources is crucial for their seamless integration with next-generation skin-like wearable and implantable biomedical systems for long-term health monitoring. Toward this goal, stretchable energy storage and conversion devices (ESCDs), including supercapacitors, lithium-ion batteries (LIBs), solar cells, and generators are now attracting intensive worldwide research efforts. The purpose of this review is to discuss the latest achievements in the development of such stretchable energy devices in the context of biomedical applications. We first review the viable strategies and methodologies of fabricating stretchable energy storage and conversion devices. Then, we focus on description of various types of soft energy devices from a materials point of view. Furthermore, we discuss the challenges and opportunities in the design of truly conformal soft energy systems, including various key parameters, such as energy density, stability, and scalability.

1. Introduction

The last several decades have witnessed tremendous advances in photolithography technologies, allowing for production of smaller microelectronic components such as transistors. This leads to innovation in the microelectronics industry, transitioning from shared computing and personal computing, to current portable computing. However, to date electronic systems remain largely based on hard and brittle materials such as silicon and metal, limiting their applications where large mechanical deformation ($\epsilon > 5\%$) is required (most of the traditional metal and semiconductive materials exhibited a mechanical deformation of $<5\%$ before failure).^[1] On the other hand, there is an increasing demand for conformal wearable or implantable electronic sensors for measurement and collection of vital biometric data from human body in real-time and in situ so that the healthcare of mankind can be better managed.^[1] One of key challenging issues for such wearable or implantable systems is how to develop sustainable energy solutions to power them in the context of biological environments. It has to

be noted that currently hot energy research is mainly tailored towards electrical cars or equivalent, in which energy density and power density are the two key parameters for pushing the limit. In contrast, in the context of wearable or implantable devices, seamless integration with biological materials and long-term durability in biological conditions are more important factors. In particular, conventional energy devices are typically in a rigid bulky or planar structure, which are neither deformable nor compliant to curved and soft biological surfaces, including tissues or organs.^[2]


It is encouraging to see that there have been considerable research efforts on stretchable and compliant energy storage and conversion systems over last five years. Several excellent review papers have

discussed flexible energy devices, either from a mechanics perspective or materials perspectives.^[3] In this context, this review article is dedicated to discuss the viability and compatibility of up-to-date energy storage/conversion devices for different biomedical applications, particularly in the emerging area of wearable and implantable biodiagnostics. We will base our discussion on the power storage and generation capability of soft power sources and the feasibility of integrating them into biomedical applications. **Figure 1** highlights the examples of several biomedical devices and the range of their typical power and voltage requirement.^[4] Typical biomedical devices including implantable radio transmitters, pacemakers, wearable glucose sensors, pressure sensors and surface electromyography (sEMG) only require a voltage of <100 mV and a power consumption of <20 μ W, which could be supplied by stretchable energy storage devices such as supercapacitors and lithium-ion batteries. Supercapacitors will not allow continuous long-term energy supplies without recharging, while the cycling stability and seamless integration of lithium-ion batteries with other soft components will pose further challenges. Wearable photovoltaic devices may become a sustainable green energy solution, but the typical energy density provided is approximately two orders of magnitude lower in diffuse light and in the absence of an external light source.^[2] Novel wearable nanogenerators based on piezoelectric and triboelectric devices can only provide intermittent energy and must be integrated with energy storage devices for continuous long-term health monitoring, which is important, especially for implantable systems (Figure 1).

We mainly cover the progress made over the past five years. Firstly, we will discuss the design principles based on either materials that stretch (MTS) or structures that stretch (STS); principles towards highly stretchable energy devices

Dr. S. Gong, Prof. W. L. Cheng
Department of Chemical Engineering
Monash University
Clayton, Victoria 3800, Australia
E-mail: wenlong.cheng@monash.edu

Dr. S. Gong, Prof. W. L. Cheng
The Melbourne Centre for Nanofabrication
Clayton, Victoria 3800, Australia

 The ORCID identification number(s) for the author(s) of this article can be found under <https://doi.org/10.1002/aenm.201700648>.

DOI: 10.1002/aenm.201700648

for biomedical applications. Then we will discuss stretchable energy storage devices including stretchable supercapacitors and batteries, which will be followed by a description of stretchable energy conversion devices. Furthermore, we will conclude this article with an overall summary and our perspectives of stretchable skin-like energy devices. Finally, we will discuss the challenges, opportunities in the assembly, and integration of energy devices with wearable and implantable sensors.

2. Design Principles

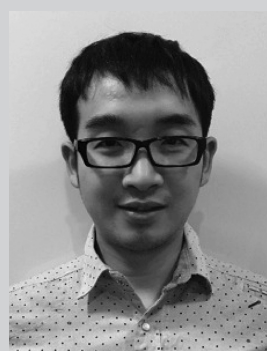
To realize conformal integration of stretchable electronic devices with human skin and tissues, there is a prerequisite to develop modulus-matching stretchable energy storage and conversion devices to integrate them seamlessly with sensors and other components with biological systems.^[38] In general, there are two viable design principles: 1) structures that stretch (STS). STS is a non-intrinsic stretchable design, which is based on the fact that a materials bending stiffness will decrease as the thickness decreases. Buckled or serpentine design can be used to achieve high stretchability by photolithography^[5] or pre-strain techniques;^[6] 2) materials that stretch (MTS). MTS is an intrinsically stretchable design. It requires the use of intrinsically stretchable materials to replace each component of traditional energy devices such as electrodes, electrolytes, and separators.^[1a] Although novel materials (e.g., carbon nanotubes, graphene, metallic nanowires) have been successfully used in MTS devices, they usually can only sustain a small strain (typically less than 10%) before cracking and/or delamination happens.^[3b] In order to overcome this limitation, STS and MTS strategies have been combined to accommodate significant deformation for wearable or implantable applications.^[1a]

2.1. Structures that Stretch

The electrodes and/or active materials are key components for stretchable ESCDs, which are required to withstand harsh mechanical deformation with stable electrical properties. By novel structural design, rigid and brittle metal and semiconductive materials ($\epsilon < 5\%$) could sustain a large strain value of $>100\%$ with stable electrical performance. To date, the following four major structural strategies for achieving stretchable electrodes and/or active materials were proposed and demonstrated: 1) buckling design, 2) serpentine design, 3) origami design, and 4) porous/textile design.

2.1.1. Buckling Design

Buckling design has become one of the most well-developed strategies to achieve the mechanical stretchability of electronic devices, due to its simple and controllable fabrication process. The buckling structure could be introduced either by mechanically pre-strain^[6] or thermal induction.^[7] Either approach allows the introduction of a different initial strain between a soft substrate layer (e.g., polydimethylsiloxane, Ecoflex) and a hard layer (e.g., metal, semiconductor, carbon based materials).^[8] Owing to the Young's modulus discrepancy between layers, periodic wavy structures could be formed upon strain release.^[9]



Shu Gong is a Research Fellow at Monash University, Australia, under the supervision of Professor Wenlong Cheng. He received his B.S. from Central South University, China, in 2011, and his Ph.D. from Monash University in 2017. At Monash University, his research interests include the development of soft electronics based on nanomaterials.



Wenlong Cheng is a Professor in the Department of Chemical Engineering at Monash University, Australia, and an Ambassador Technology Fellow in Melbourne Centre for Nanofabrication. He earned his B.S. from Jilin University, China, in 1999, and his Ph.D. from Chinese Academy of Sciences in

2005. He held positions in the Max Planck Institute of Microstructure Physics and the Department of Biological and Environmental Engineering of Cornell University before joining the Monash University in 2010. His research interests lie at the nano-bio interface, particularly addressing plasmonic nanomaterials, DNA nanotechnology, nanoparticle anticancer theragnostics, and electronic skins.

This kind of buckling design has been applied to a variety of rigid materials including metal^[10] and semiconductors,^[6,11] in both a coplanar manner and a non-coplanar manner (**Figure 2a**). The buckling film can accommodate large tensile (up to 100%), compressive (up to 25%), and bending (with a curvature radius down to ≈ 5 mm) strain to maintain the integrity of functional devices.^[11] The wavy design was first exploited to fabricate stretchable energy devices in 2009, where a coplanar, wavy geometry, single-walled carbon-nanotube microfilms-based supercapacitor was reported (**Figure 2b**).^[12] The resultant device showed no obvious capacitance degeneration when subjected to 30% applied strain. Thereafter, this strategy has been applied to a variety of novel active materials, including carbon nanotubes (CNTs),^[13] graphene,^[14] and conductive polymers,^[15] for the construction of uniaxial stretchable energy devices. The above strategy was further extended to biaxial pre-strain to generate biaxial wavy geometry (**Figure 2c**), which could provide stretchability along all in-plane directions.^[16] Based on this concept, crumpled patterns of graphene paper film were demonstrated with extremely large pre-strains up to 400% (**Figure 2d**).^[17] Supercapacitor electrodes based on the crumpled graphene papers exhibit a unique combination of high stretchability (e.g., linear strain, 300%; areal strain, 800%) and high electrochemical performance (e.g., specific capacitance, 196 F g^{-1}).^[18] Other morphologies, such as hierarchically wavy geometry^[19]

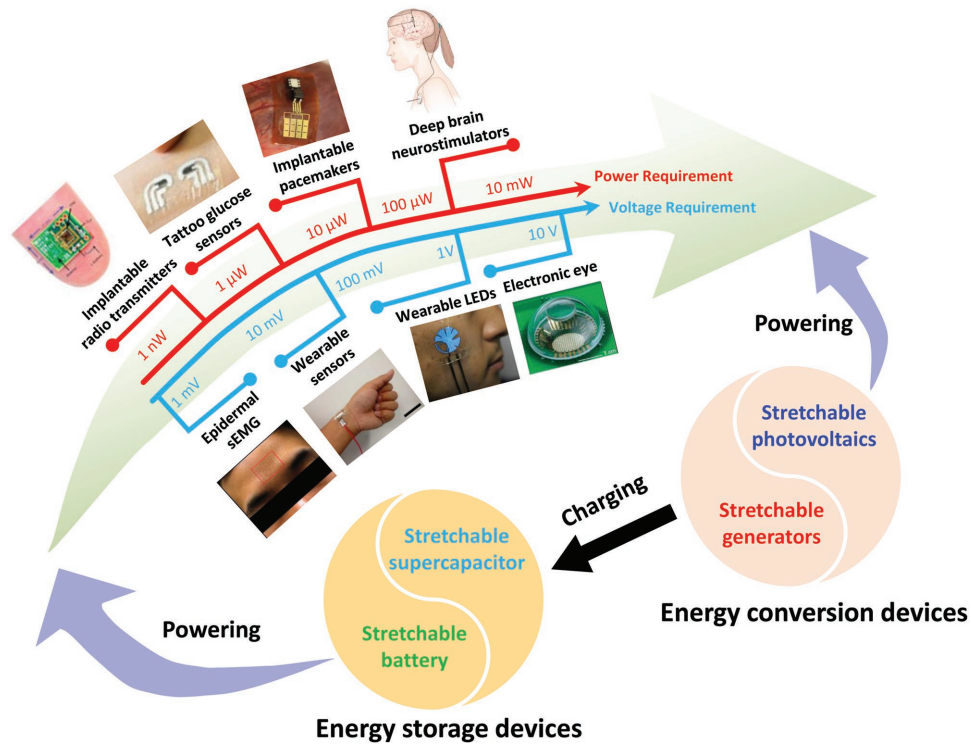


Figure 1. Order of magnitude of typical power and voltage requirements of biomedical devices and the integration between energy-storage/conversion devices with these data-collection devices. Image “implantable radio transmitters”: Reproduced with permission.^[4a] Copyright 2012, Nature Publishing Group. Image “tattoo glucose sensors”: Reproduced with permission.^[4c] Copyright 2014, American Chemical Society. Image “implantable pacemakers”: Reproduced with permission.^[4b] Copyright 2014, National Academy of Sciences, U.S.A. Image “deep brainneurostimulators”: Reproduced with permission.^[4f] Copyright 2012, American College of Neuropsychopharmacology. Image “epidermal electronics”: Reproduced with permission.^[4d] Copyright 2015, Wiley-VCH. Image “wearable sensors”: Reproduced with permission.^[4e] Copyright 2014, Nature Publishing Group. Image “wearable LEDs”: Reproduced with permission.^[4g] Copyright 2016, American Association for the Advancement of Science. Image “electronic eye”: Reproduced with permission.^[4h] Copyright 2008, Nature Publishing Group.

(Figure 2e) and wrinkle geometry^[20] (Figure 2f), were introduced in recent years to further extend the stretchability of electrode materials with high quality factors (Q , the percent strain divided by the percent resistance change). It is noted that conductive electrodes with high quality factors can be stretched to great extents without significantly changing conductivity, which could enable the application of superelastic electrodes for stretchable supercapacitors or batteries.^[19]

The buckling approach makes brittle and rigid materials bendable and stretchable because the overall system can be stretched reversibly to large levels of strain, without fracturing the material through changes in the wavelength and amplitude of the wavy structures.^[3b] A detailed theoretical analysis of the buckling wavelength (λ) and amplitude (A) of wavy ribbon structures has been summarized in several review papers.^[21] In the range of small strains, λ and A are determined through the minimization of total strain energy:

$$\lambda = 2\pi h_f \left(\frac{\bar{E}_f}{3\bar{E}_s} \right)^{\frac{1}{3}}, A = h_f \sqrt{\frac{\varepsilon_{pre}}{\varepsilon_c} - 1} \quad (1)$$

$$\varepsilon_c = 0.25 \left(\frac{3\bar{E}_s}{\bar{E}_f} \right)^{\frac{2}{3}} \quad (2)$$

where ε_c is the critical strain for the buckling, h_f is the film thickness, E is the plane-strain moduli, and f and s denote film and substrate, respectively. Equation (1) and (2) indicate a constant wavelength independent of the pre-strain, and agree reasonably well with experimental measurements only when the pre-strain is rather small (e.g., <5%).

In the range of large strains, the elastomeric polydimethylsiloxane (PDMS) substrate becomes non-linear, and thus the pre-strain-dependent buckling wavelength and amplitude are described as follows:^[21]

$$\lambda = \frac{\lambda_0}{(1+\varepsilon_{pre})(1+\xi)^{1/3}}, A = \frac{A_0}{(1+\varepsilon_{pre})(1+\xi)^{1/3}} \quad (3)$$

$$\xi = \frac{5}{32} \varepsilon_{pre} (1+\varepsilon_{pre}) \quad (4)$$

where λ_0 and A_0 are the wavelength and amplitude given by Equation (1), respectively. The analytic models to study the effects of finite ribbon width and bilayer substrate were also reported.^[22]

2.1.2. Serpentine Design

Serpentine bridge–island design is another efficient strategy to fabricate stretchable energy devices, in which rigid island

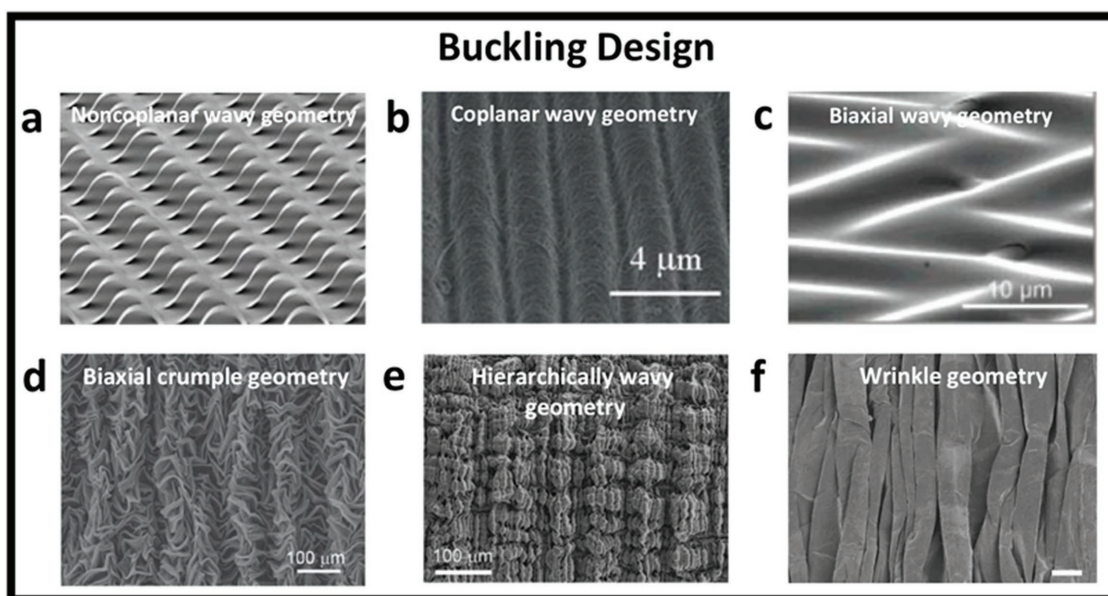


Figure 2. a) Scanning electron microscopy (SEM) images of a non-coplanar Si ribbons. Reproduced with permission.^[11] Copyright 2006, Nature Publishing Group. b) SEM images of a coplanar CNT film with wavy geometry. Reproduced with permission.^[12] Copyright 2009, Wiley-VCH. c) SEM images of a Si film with biaxial wavy geometry. Reproduced with permission.^[16a] Copyright 2007, American Chemical Society. d) SEM images of a graphene film with biaxial crumple geometry. Reproduced with permission.^[17] Copyright 2013, Nature Publishing Group. e) SEM image of a CNT film with hierarchically wavy geometry. Reproduced with permission.^[19] Copyright 2015, American Association for the Advancement of Science. f) SEM image of a CNT paper with wrinkled geometry. e–f) Reproduced with permission.^[20] Copyright 2015, Nature Publishing Group.

materials (e.g., Si) were interconnected with stretchable serpentine conductive patterns (e.g., by gold stripes).^[5] Such serpentine interconnects have much lower effective stiffness when compared to rigid active “bridge” components, which could undertake most of deformation upon stretching to ensure the functionality of the whole device.^[3g]

Similar to the buckling design, the serpentine interconnect can be coplanar^[23] or non-coplanar^[5,24] to the elastomeric substrate. Coplanar configuration enables fully bonded serpentine interconnects with stretchable substrates. The stretchability of this design is highly related to the geometry of the pattern and the stiffness of the substrate. The localized strain is significantly reduced by applying narrow metallization strips and low elastic modulus of the substrate.^[23]

The pre-strain techniques can be combined with serpentine design of metal electrodes, which yielded a significantly enhanced (more than two times) stretchability to >100%.^[25]

Compared to coplanar design, non-coplanar configuration allows the serpentine interconnect partially bonded or completely non-bonded to the elastomeric substrates, which involves not only in-plane, but also out-of-plane deformations. This configuration could lead to ultra-stretchable electrodes that offer biaxial stretchability up to ≈170% (Figure 3a,b).^[24] In the non-coplanar bridge-island system, mechanics models of both bridge and island can guide and optimize the design of patterns.^[26] For the bridge, the maximum strain (ϵ_{bridge}^{max}) is given by:

$$\epsilon_{bridge}^{max} = 2\pi \frac{h_{bridge}}{L_{bridge}^0} \sqrt{\frac{\epsilon_{pre}}{1 + \epsilon_{pre}}} \quad (5)$$

where h_{bridge} is the thickness of interconnect, L_{bridge}^0 is the distance between islands before releasing, and ϵ_{pre} is the pre-strain. For the island, the maximum strain (ϵ_{island}^{max}) is obtained as:

$$\epsilon_{island}^{max} = \frac{\epsilon_{island}^{max} \times E_{bridge} h_{bridge}^2}{(E_{island} h_{island}^2)} \quad (6)$$

where E_{bridge} is the Young’s modulus of the bridge, E_{island} is the Young’s modulus of the island, and h_{island} is the thickness of island. The thickness of the bridge is generally much smaller than the thickness of the islands, which could explain the negligible strain change of islands under stretching. Therefore, the deformation strain absorbed through the motions of the out-of-plane interconnects avoids any significant effect on the islands.^[3b] From the above two equations, the device stretchability of such a design could be obtained via increasing the length of bridge and decreasing the length of island. However, there is always a tradeoff between a high level of stretchability and high areal coverage of active devices. This is especially vital for stretchable ESCDs, as low areal coverage of active materials means low energy storage or conversion efficiency. To address this problem, a self-similar design was demonstrated to make full use of a limited space of bridging electrodes by increasing the fractal order, as shown in Figure 3c,d. The stretchable lithium-ion battery arrays using the fractal serpentine bridge–island design exhibited a high stretchability of ≈300% simultaneously with enhanced areal surface of active materials (≈50%), which enables full attachment onto human joints at bending states.^[27] The fractal layout used n^{th} order serpentine interconnects, where the scale of the $(n-1)^{\text{th}}$ order interconnect was reduced.

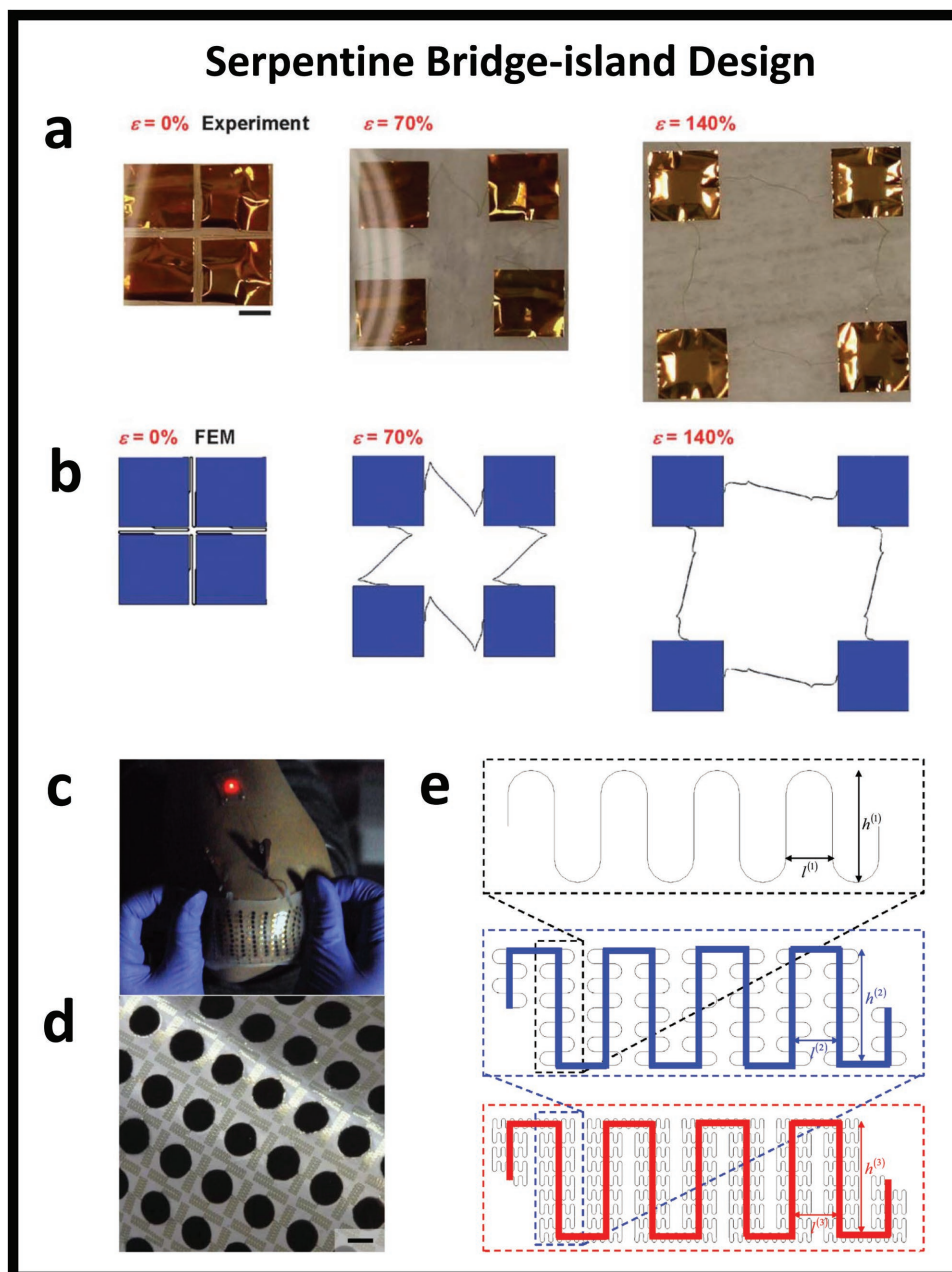


Figure 3. a) Experimental and b) numerical results of the deformation modes under different levels of biaxial strains. Scale bar: 1 mm. Reproduced with permission.^[24] Copyright 2013, The Royal Society of Chemistry. c) Optical images of the LIB pads and self-similar interconnects on a Si wafer. Scale bar: 2 mm. d) Optical images of the stretchable LIB attached onto human knee. Reproduced with permission.^[27] Copyright 2013, Nature Publishing Group. e) Schematic illustration on the geometric construction of the self-similar serpentine interconnect. Reproduced with permission.^[28] Copyright 2013, Elsevier Ltd.

The fractal patterns were 90 rotated and multiple copied following the trace of original geometry (Figure 3e). An analytical model was developed through establishing the recursive formulae at different fractal orders.^[28] The analytic flexibility components are more than doubled for each n increase by 1, which was further validated by finite element analysis.^[28] Fully bonded fractal interconnects with various layouts were also studied, representing important strategies for hard-soft materials integration.^[29]

2.1.3. Origami Design

Origami is an ancient art of paper folding that can turn a sheet of paper into compact, deformable, three-dimensional (3D) structures through high degrees of folding along predefined creases. The origami design of stretchable batteries was recently reported through Miura folding, shown in Figure 4a.^[30] Many identical parallelogram faces were connected by ‘mountain’ and ‘valley’ creases. Depending on the difference in

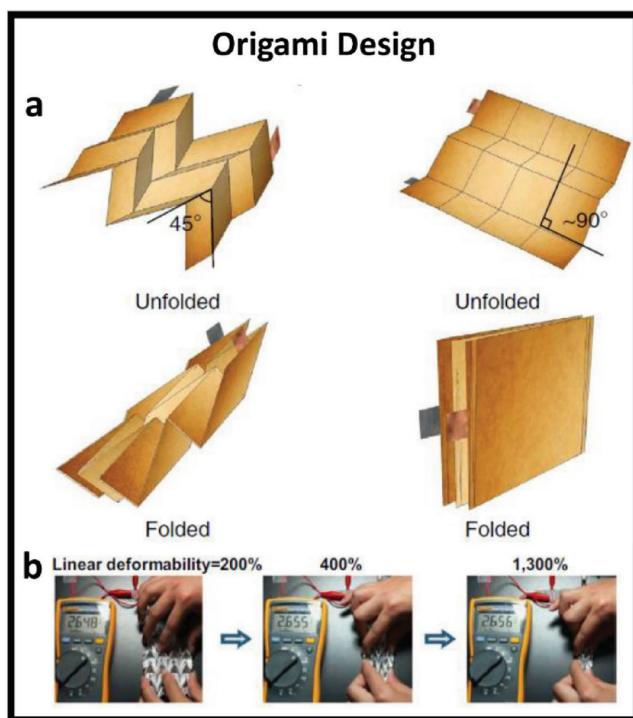


Figure 4. a) Two examples of origami LIBs using Miura folding. 45° Miura folding (left) and 90° Miura folding (right). b) Photograph of linear deformation (folding and unfolding) of an origami LIB while it was connected to a voltmeter. Reproduced with permission.^[30] Copyright 2014, Nature Publishing Group.

angles between adjacent ‘mountain’ and ‘valley’ creases, the Miura folding could be either almost completely compressible in one direction (left of Figure 4a, 45° Miura folding)^[30,31] or collapsible in two directions (right of Figure 4a, 90° Miura folding).^[32] Lithium-ion batteries using 45° Miura folding were examined and showed steady output voltage performances, even up to 1340% linear deformability with respect to their completely compressed states (Figure 4b).^[30] Folded batteries with 90° Miura folding also displayed a $\approx 14 \times$ increase in areal energy density compared to the planar versions with a 5×5 cell.^[32] Other configurations of paper based on slinky origami design^[33] or kirigami design^[34] have been applied to the construction of stretchable nanogenerators,^[33] supercapacitors,^[34a] and lithium-ion batteries.^[34b]

The effective mechanical properties of origami structures have been studied through analytical modelling.^[35] Under external mechanical loadings, the parallelogram faces themselves usually remain undeformed, since the folding and unfolding of the creases maintain the faces in a rigid configuration. Therefore, the deformability is mainly prescribed by the creases, and the origami patterns do not experience large strain except at the crease locations. As a result, the curvature radius of the creases becomes critical in the origami design to reduce the strain level for avoiding fracture or plastic yielding. Strategies such as using stretchable material^[30] and stretchable structural design^[31] have been adopted to the creases of origami patterns to achieve good foldability while maintaining high electrical conductivity.

2.1.4. Textile/Porous Design

3D textiles or 3D porous structures are superior candidates for energy devices, as they possess high surface-to-volume ratios essential for enhancing energy/power densities.^[36] With appropriate material choices, such structures can also be stretched up to 200% without mechanical fracture.^[37]

Much work has been done to evaluate the elastic properties of textile materials via theoretical and experimental studies.^[38] In general, stretchability of a textile is highly dependent on the fibre materials of choices, spinning methods of yarns, and weaving/knitting methods of textiles. Figure 5a shows a typical interlaced yarn with a helical coiled structure,^[39] which consists of several individual fibres, as indicated in Figure 5b,^[38a] the length of the fibre is described as: $L = 2\pi r n \tan \theta$ (Figure 5c), where L , r , n and θ are the fibre length, radius, number of coils, and pitch angle, respectively. When the pitch angle (θ_0) is fixed, the maximum strain stretch ratio (ν_{sr}^{max}) is given by:^[3b]

$$\nu_{sr}^{max} = \frac{2\pi r n}{L \cos \theta_0} = \frac{1}{\sin \theta_0} \quad (7)$$

It has to be noted that the calculated stretchability using the above model is only for yarns. The knitted textile based on helical coiled yarns may provide additional stretchability to the hierarchical structures. Stretchability of textile structure may be further improved by pre-straining a textile before active materials deposition,^[40] or twisting yarns onto elastomeric core fibres.^[41]

Porous structures from elastomeric materials (e.g., PDMS and polyurethane) constitute an additional viable strategy for stretchable energy devices. As shown in Figure 5d, active materials deposited on the conventional electrode will crack under high strains due to their rigid nature. However, when active materials are deposited into porous elastomers, this issue can be avoided.^[42] Also, the porous electrodes can accommodate strain in all directions, whereas most buckling designs or helically coiled spring designs can only subject to stretch unidirectional.

2.2. Materials that Stretch (MTS)

Novel materials provide an alternative route to stretchable electronics since they can be stretched intrinsically. The intrinsically stretchable materials, including conductors, semiconductors, insulators, solids, gels, and liquids, have been applied for stretchable ESCDs.

2.2.1. Intrinsically Stretchable Materials for Stretchable Electrodes

Traditional electrodes and active materials for energy storage and conversion devices mainly include: 1) carbon-based materials; 2) conductive polymer-based materials; and 3) metal-based materials. However, most of them are not intrinsically stretchable due to their high rigidity and brittleness. For example, carbon black particles have relatively poor connectivity

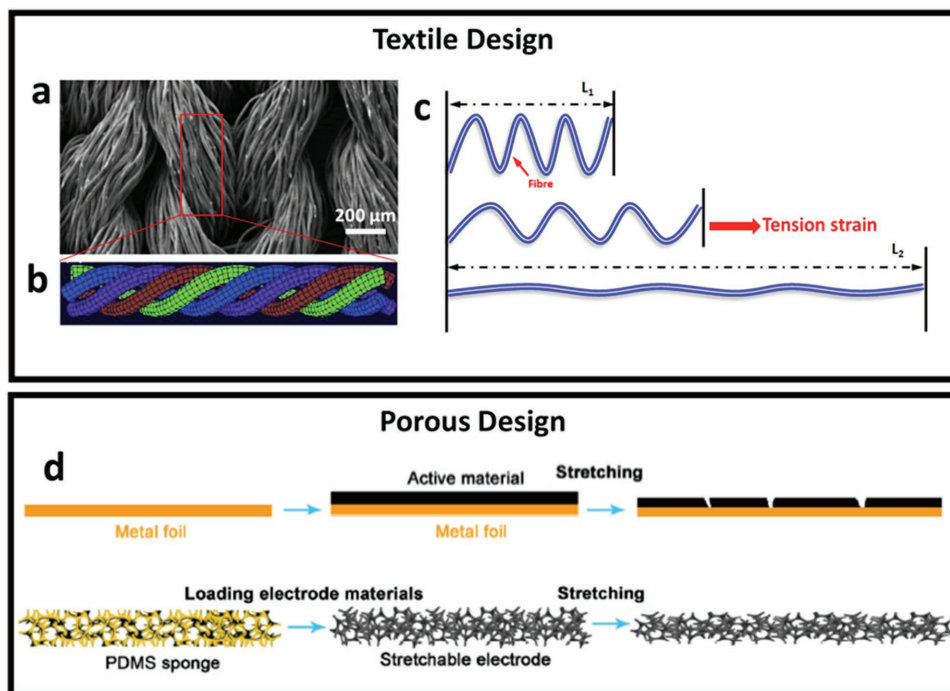


Figure 5. a) SEM image of a typical textile based stretchable electrode. Reproduced with permission.^[39] Copyright 2016, Wiley-VCH. b) A typical coaxial yarn geometry. Reproduced with permission.^[38a] Copyright 2012, Elsevier Ltd. c) Stretch ratio of helical coiled structure. d) Schematic illustration for the comparison of the conventional electrode using metal foil and the stretchable electrode based on the PDMS sponge. Reproduced with permission.^[42] Copyright 2016, Wiley-VCH.

and cannot well maintain their overall structural integrity, and hence conductivity upon stretching.^[3a] One dimensional nanomaterials offer unique advantages due to their inherent high-aspect-ratio structural feature, in conjunction with superior mechanical, electrical, and optical properties, which enables the construction of a percolation network with low consumption of materials, yet high stretchability.^[43] In detail, CNTs and metal nanowires are considered as excellent candidates for stretchable electrodes and active materials of stretchable ESCDs. In 2011, a transparent, conducting, single-walled carbon nanotube (SWCNT) film accommodating strains up to 150% without pre-strain was demonstrated.^[44] This is attributed to the spring-like structure of nanotubes produced during stretching. Furthermore, a design of horizontally aligned CNTs transferred on PDMS was introduced as stretchable electrodes for supercapacitors. Such supercapacitors showed negligible capacitance changes upon stretching up to 240%.^[45] During tensile strain, most of aligned CNTs are slipped to each other, instead of cracking and debonding, which is important for maintaining conductivity and capacitance when being stretched. Such aligned CNT sheet could also be wrapped onto elastomeric fibres with a pre-strain of only 100%, to achieve superior stretchability of over 400% (Figure 6a).^[46] The resistance changes upon stretching are highly dependent on the helical angle between the aligned CNT sheet along the axial direction of the fibre (Figure 6b,c). Optimized stretchability is achieved with a helical angle of 80°, where the resistance variances are within 70% at strains of ≈400%.

Ag nanowire is considered as an excellent candidate for stretchable and potentially transparent electrodes, and has

been widely chosen as the current collectors of flexible photovoltaics devices and nanogenerators. For example, percolating silver nanowire (AgNW) films on stretchable Ecoflex substrates have been reported to have excellent stretchability and resistance retention upon stretching.^[47] Similar properties have been observed by high quality copper nanowires, which are earth-abundant and much cheaper than AgNWs.^[48] In addition, ultrathin gold nanowires (AuNW) with a diameter of only 2 nm and a high aspect ratio of >10000 exhibited inherent curved morphologies, emerging as intrinsically stretchable building blocks for stretchable electronics, including wearable sensors,^[4e,49] transparent electrodes,^[50] and stretchable supercapacitors.^[51] In particular, the self-assembled transparent ($T = 90\%$ at a wavelength of 550 nm) AuNWs film (≈ 8 nm) could allow a stretchability of 50% with reversible resistance changes of only 45%, due to a strain induced wrinkle structure (Figure 6d,e).^[51] Supercapacitors based on such electrodes provide a high transparency of >80%, as well as a stable capacity with stretchability up to 30%, which are promising for the application of invisible and wearable energy devices.

Apart from 1D nanomaterials, graphene and conductive polymers have also been used for the fabrication of ESCDs with intrinsic stretchability. In 2009, stretchable graphene electrodes were first reported using high-quality graphene transferred from Cu foil to a PDMS substrate.^[52] The stretchable graphene electrodes can work efficiently under uniaxial strain up to 30%, with resistance variances within 10%. As the most commonly used conductive polymer, PEDOT:PSS (poly(3,4-ethylenedioxythiophene):polystyrene sulfonate) has been reported for stretchable solar cells with stable performance at stains up to 20%.^[53]

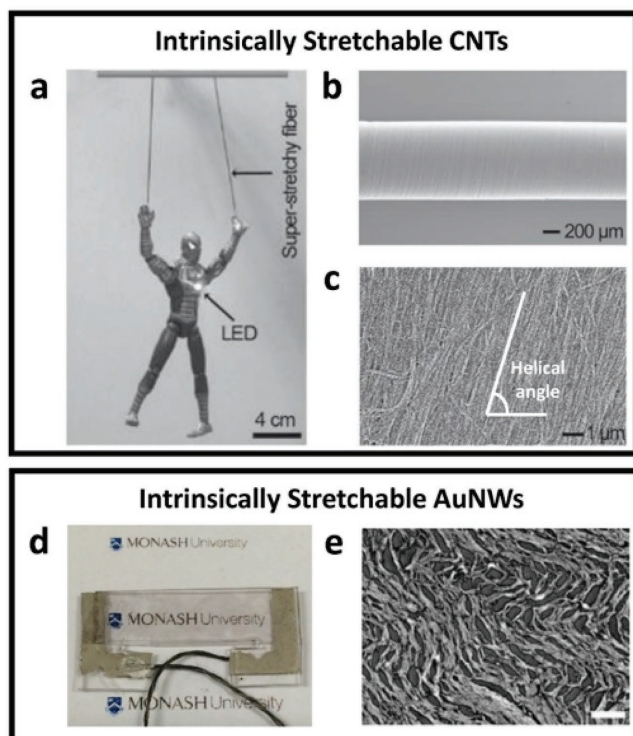


Figure 6. a) Photograph of the CNT elastic fiber electrode to power a light-emitting diode during stretching. b,c) SEM images of the aligned CNT sheet and aligned CNT/PANI sheet, respectively. Reproduced with permission.^[46] Copyright 2015, Wiley-VCH. d) Photograph of the transparent stretchable AuNWs supercapacitor. e) SEM images of the stretch-aligned AuNWs film after cyclic strain (30%) of 5000 times. Scale bar: 500 nm. Reproduced with permission.^[51] Copyright 2016, Wiley-VCH.

Although a variety of nanomaterials showed greater intrinsic stretchability than traditional active materials due to their novel percolating structures, efforts still need to be devoted to enhance their conductivity and electrical stability. For instance, the resistance of aligned CNT fibre electrodes are in the range of 1 to 4 k Ω cm⁻¹, which will be further increased to \approx 10 k Ω cm⁻¹ upon 400% strain. This value is >1000 times larger than the traditional carbon grease or carbon black electrodes used in energy storage devices. As a result of low conductivity, low specific capacitances of the final devices are expected. Some strategies had been proposed to significantly reduce their resistances by lengthening the 1D nanomaterials^[47,54] or making a pressurized rolling post-treatment.^[55] In addition, the combination of structural design with novel, intrinsically stretchable materials could enable almost constant electrical properties of electrodes during stretching.

2.2.2. Intrinsically Stretchable Materials for Stretchable Electrolytes

An intrinsically stretchable ESCD requires each component, including electrodes, separator, and electrolyte, to be stretchable. In this case, exploring novel electrolyte materials that are intrinsically elastic is equally important. Liquid electrolytes could perfectly accommodate the deformation of solid encapsulates until failure, due to significantly lower Young's modulus

of liquid. However, the encapsulation of liquid electrolytes in wearable ESCDs is challenging, due to potential safety issues such as leakage, flammability, and poor chemical stability while energy devices are being used.^[56] Therefore, considerable efforts have been made to replace liquid electrolytes with gel and solid ionic electrolytes.

Stretchable phosphoric acid (H₃PO₄)/polyvinyl acetate (PVA) and sulfuric acid (H₂SO₄)/PVA gel electrolytes are the most commonly used electrolytes for stretchable supercapacitors. The conductivity and mechanical properties of such electrolytes is highly dependent on the polymer molecular weight of PVA and its weight ratio to the acid. A highly stretchable H₃PO₄/PVA polymer electrolyte with optimized PVA:H₃PO₄ weight ratio of 1:1.5 was reported, which showed a high conductivity of 3.4 \times 10⁻³ S cm⁻¹ and a high fracture strain at 410% elongation.^[57] Stretchable supercapacitors based on buckling conductive polymer film and the resultant electrolytes showed good capacitance retention of 94.5% under 30% strain, and capacitance retention of 81% after 1000 stretch/release cycles. However, strong acids in the gel electrolytes may also trigger safety issues. An alternative choice is to use ionic liquids as additive for safe gel or solid electrolytes. In 2013, A gum-like hybrid electrolyte was presented with improved safety and stretchability.^[58] This hybrid electrolyte consists of a double percolation network structure, in which a percolation network of a liquid electrolyte is supported by a network of solid particles and a strong entanglement network of polymer electrolyte (polyethylene oxide with LiClO₄). The gum-like hybrid electrolyte with liquid electrolyte content of ca. 50 wt% showed a high ionic conductivity (ca. 3 \times 10⁻⁴ S cm⁻¹ at room temperature) and arbitrary deformability, with minimized influence on its conductivity, which are desirable for stretchable batteries application. In addition, when the temperature reached the melting point of the wax particles, the ionic conductivity of electrolytes decreased in order to cease the electrochemical reaction. Consequently, the working temperature of batteries can remain in a safe range. Except for gum-like electrolytes, stretchable solid polymer electrolytes have also been demonstrated.^[59] The solid polymer electrolytes were comprised of lithium bis(fluorosulfonyl) imide (Li[N(SO₂F)₂], LiFSI) and polymeric ionic liquid, which could be stretched up to more than 5 times of its original length without breaking. The maximum ionic conductivity for the solid polymer electrolyte is 1.4 \times 10⁻⁵ S cm⁻¹ at 30 $^{\circ}$ C, with much lower interface resistances for Li symmetric cell than those using LiTFSI/P[C₅O₂N_{MA,11}]/TFSI electrolyte.

In addition, the combination of superior self-healability and stretchability is important for wearable and implantable energy devices. Conventional PVA-based acidic electrolytes are intrinsically neither self-healable nor highly stretchable. Recently, an electrolyte consisting of polyacrylic acid dually crosslinked by hydrogen bonding and vinyl hybrid silica nanoparticles, provides a solution to the intrinsic self-healability and high stretchability.^[20] The supercapacitors with this stretchable electrolyte and CNT-paper wavy electrodes could be stretched up to 600% strain, and retain capacitance even after 20 cycles of breaking/healing. The highly stretchable supercapacitors with self-healing features indicate a wide range of applications for powering wearable electronics.

3. Stretchable Energy Storage Devices

3.1. Stretchable Supercapacitors

Supercapacitors have attracted considerable attention in recent years due to their fast charge–discharge rate, high power density, moderate energy density, and long operation life. Based on their different energy storage mechanisms, supercapacitors are divided into three types: electrochemical double layer capacitors (EDLCs), pseudocapacitors, and hybrid capacitors. A typical EDLC stores electrical energy by electrostatic accumulation of charges at both the interface between the electrode and electrolytes. Meanwhile, the energy storage of pseudocapacitors is achieved through reversible and fast redox reactions. Hybrid capacitors are combinations of an EDLC or pseudocapacitor, which utilize both Faradaic and non-Faradaic processes to store charges. Generally, supercapacitor are mainly composed of three parts: electrodes/current collectors, electrolytes, and separators. The structure and electrochemical properties of electrodes have a critical impact on the performance of a supercapacitor, which have been extensively studied in several review paper.^[3c,e,60] Traditional EDLC electrode materials include activated carbon particles, carbon black, and carbon grease, while metal oxides/hydroxides and electrically conducting polymers are pseudocapacitor electrode materials. Typically, EDLC electrode materials have a better charge–discharge rate, higher power density, and longer operation life than pseudocapacitor electrode materials due to the high conductivity and stability of carbon-based materials. However, EDLC electrode materials generally show a lower capacitance and energy density than pseudocapacitor electrode materials. This is because reversible oxidation/reduction reaction(s) will occur at the electrode/electrolyte interface of the pseudocapacitor, giving 10–100 times more capacitance than that of pure carbon-based EDLC.^[61]

To date, various novel materials with intrinsic stretchability (e.g., carbon nanotubes, carbon nanofibers, graphene, and

metal nanowires)^[18,45,46,51] and structural designs (e.g., wire configuration,^[62] film configuration,^[12] and textile configuration)^[37] have been proposed for the purpose of developing stretchable and implantable supercapacitors. We will discuss several viable configurations.

3.1.1. 1D Wire-Based Configuration

Wire-based stretchable supercapacitors have been developed rapidly in recent years, due to their lightweight and easy integration with smart clothes.^[3e] Flexible wire-like power sources can be woven into various clothes, which showed excellent compatibility with wearable electronics. There are mainly two configurations for wire-shaped stretchable supercapacitors: coaxial design^[46,62] and non-coaxial design^[41,63] (Figure 7). The first coaxial, stretchable, wire-shaped supercapacitors was developed in 2013 (Figure 7a).^[62] The stretchability was achieved by wrapping an aligned CNT sheets layer, a thin gel electrolyte layer, and another CNT sheets layer coaxially onto elastic fibres (Figure 7b). This design could maintain high contact areas and low contact resistance between the electrode and electrolytes, resulting in a high specific capacitance of 19.2 F g⁻¹. This could be further enhanced to 41.4 F g⁻¹ by introducing OMC components among aligned CNTs. Conductive polymers such as PEDOT:PSS^[63a] and polyaniline (PANI)^[46] were also electrodeposited onto such coaxial CNT film to improve the specific capacitance. For instance, new fibre-shaped, stretchable supercapacitors based on an aligned CNT/PANI composite electrode and stretchable gel electrolyte onto Ecoflex elastic wires has been recently demonstrated.^[46] The resultant supercapacitor could be stretched up to 450% strain with almost no change in performance, indicating good stretching stability of this design. More importantly, a high specific capacitance of about 79.4 F g⁻¹ was well maintained by stretching under a 300% strain for 5000 cycles with fiber-shaped design. The

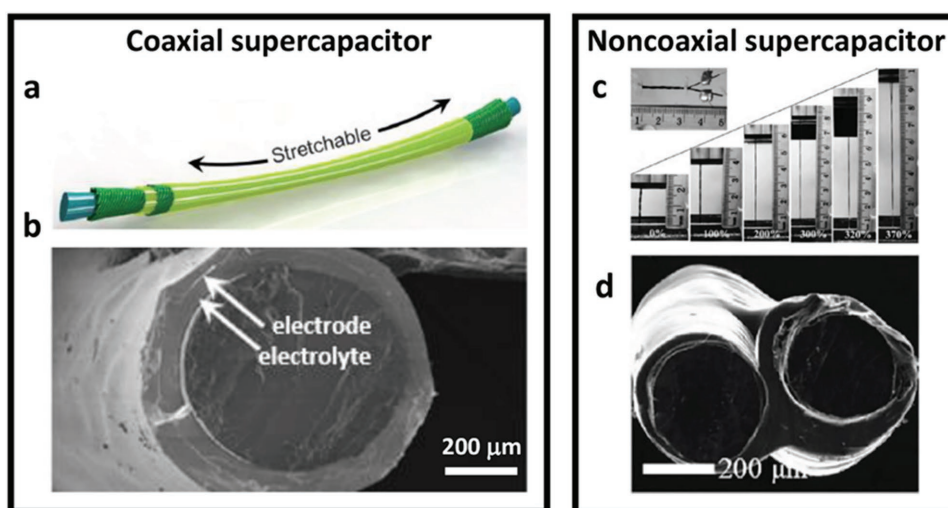


Figure 7. a) Scheme of a 1D wire-like coaxial stretchable supercapacitor. b) Cross-sectional SEM image of the supercapacitor with two CNT-based electrodes and gel electrolyte in between. Reproduced with permission.^[62] Copyright 2013, Wiley-VCH. c) Photographs of a 1D wire-like twist stretchable supercapacitor stretched with different strain (up to 370%). d) Cross-sectional SEM image of the supercapacitor with two CNT-wrapped electrodes, gel electrolyte in between. Reproduced with permission.^[63a] Copyright 2015, Wiley-VCH.

specific capacitance retention of the resultant device is higher than 95% after 100 stretching cycles at 75% strain, demonstrating excellent stability. Non-coaxial design involves two separate wire-based electrodes twisted or aligned together, with an electrolyte in between. In 2015, a twisted supercapacitor was introduced with high stretchability up to 350% strain (Figure 7c,d).^[63a] The wrinkled super stretchable electrode was fabricated by wrapping continuous CNT thin film around pre-stretched elastic wires (64% polyester and 36% polyurethane). Interestingly, the capacitance for the device based on the bare CNT-wrapped elastic wire electrodes increased by 13% as the tensile strain increased from 0 to 250%, presumably because of the strain-induced enhancement in the contact between the two twisted electrodes upon stretching.^[62,63] Further stretching (250–350%) caused a slight decrease in the capacitance, though it was still 10% higher than the initial capacitance. Graphene microfibers has also been chose as electrode materials for 1D wire-based stretchable supercapacitor.^[64] Such an all-graphene core–sheath fibre is composed of a core of graphene fibre with a sheath of 3D, porous, network-like graphene framework. This hierarchical hybrid structure showed both high electronic conduction of the core graphene fibre and high surface areas of 3D porous sheath. The fibre supercapacitors comprise two intertwined electrodes, and can be conveniently woven into a textile for wearable electronics. Similar designs, such as a coiled structure,^[65] have also been used for stretchable CNT-based supercapacitors, with stable electrochemical performance up to 150% strain.

In 2015, a super-stretchable conducting fibre with stretchability as high as 1320% was presented using CNT sheets oriented in the wire direction on stretched rubber wire cores.^[19] A hierarchical two-dimensional buckling core–sheath structure was formed by superhigh pre-strain. The resulting structure exhibited distinct short- and long-period buckling that occurred reversibly out of phase in the axial and belt directions, enabling a resistance change of less than 5% under a 1000% strain. Supercapacitors based on this electrode are insensitive to strain over an applied tensile strain range between 0% and 300%.^[66]

3.1.2. 2D Film-Based Configuration

The 2D film based stretchable supercapacitors could be realized by a wavy or buckled structure with a pre-strain strategy. The first wavy, stretchable supercapacitor was reported in 2009 with two sinusoidal SWNT films as the stretchable electrodes.^[12] SWNT film was firstly fabricated on the pre-stretched elastomeric PDMS substrate. A sinusoidal wavy pattern could be formed after releasing the substrate, owing to a mechanical mismatch between the relatively stiff SWNT film and the compliant PDMS substrate (Figure 8a). After assembling two sinusoidal SWCNT film electrodes with gel electrolyte, the device could withstand stretchability of 30%, with no significant change in the cyclic voltograms of the stretchable supercapacitors. The specific capacitance could be maintained by >95% under 30% strain up to 1000 charge–discharge cycles, indicating excellent cycling stability of this design. It has to be noted that the stretchability of supercapacitors based on such post-deposited CNT film is only ≈30%, which limits their

applications for powering wearable electronics. To overcome this, a highly stretchable supercapacitors by directly growing SWCNT films with continuous reticulate architecture on pre-stretched PDMS was presented.^[13a] The as-fabricated SWCNT electrodes could be stretched under a strain of 140% without the significant change of the resistance, benefitting from the continuous reticulate architecture which has a higher strain tolerance than that of post-deposited SWCNT films.^[67] Their electrochemical performance remained constant under 120% strain in the static state of stretching. Asymmetric stretchable supercapacitors were also designed with this strategy, while MnO₂/CNT and Fe₂O₃/CNT wrinkled macrofilms were applied for the electrodes of the supercapacitor (Figure 8b–d) with wide voltage window (0–2V) and high energy density (45.8 W h kg⁻¹).^[68]

Graphene has also been frequently used in stretchable supercapacitors in thin film configurations.^[17,18,69] In 2013, crumpled-graphene papers were introduced to prepare stretchable electrodes for high performance supercapacitors.^[17] The stretchable electrodes were obtained by transferring graphene paper onto the pre-stretched elastomer film along one or two directions, sequentially. The stretchable electrodes based on the crumpled graphene papers exhibited a high level of stretchability, with linear strain of 300% and areal strain of 800%, and negligible changes in resistance. At the device level, the crumpled graphene-paper-based supercapacitors have demonstrated specific capacitances in the range of 28 to 49 F g⁻¹, with large deformability; up to 150% uniaxial strain and 300% areal strain.^[18] The buckling structural design imparts stretchability to electrodes, mainly because the wavy structure can effectively avoid rupture and crack from conductive film.

Most of the electrochemical studies of stretchable supercapacitors were conducted under static states; however, on-body biomedical electronics needs to have a stable energy supplier under dynamic deformations. This was addressed in a recent report on a dynamically stretchable supercapacitor using buckled SWCNT macrofilms as the electrodes, an electrospun membrane of elastomeric polyurethane as the separator, and an organic electrolyte.^[70] The stretchable supercapacitors show excellent cyclic stability under electrochemical charge/discharge during in situ dynamic stretching/releasing from 0% to 31.5% strain. The slight variance on the capacitive performance under dynamic stretching is found to be within ≈2%, which is affected mainly by the ion-diffusion process.

In addition, invisible skin-attached electronics have attracted great attention in recent years for personal aesthetic purposes. Such devices are required to be not only stretchable and wearable to human skin, but must also have transparent electrodes to make it fully invisible. However, there is a trade-off between highly transparent and highly stretchable, as high optical transparency requires very thin conductive film as stretchable electrodes, which will inevitably cause cracking or breakage of the thin film when a high level strain is applied.^[51] To address this challenge, wrinkled transparent graphene^[14,71] and CNT^[72] electrodes were used for the construction of stretchable and transparent supercapacitors. For example, a laminated ultrathin graphene film was introduced as stretchable and transparent electrodes for supercapacitors.^[71] Optical transmittance of up to 72.9% at a wavelength of 550 nm and stretchability of 40% were achieved. The specific capacitance showed no degradation,

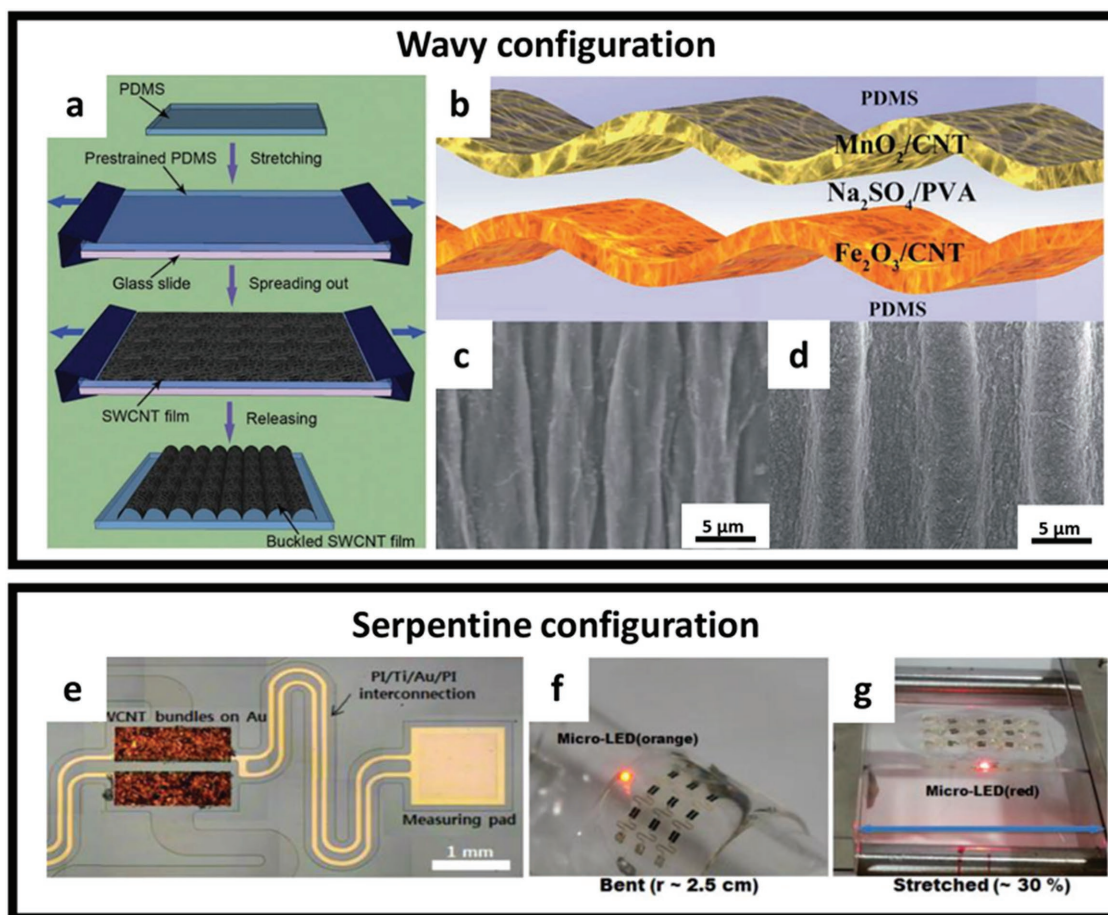


Figure 8. a) Scheme of the fabrication process for periodic buckled stretchable electrode. Reproduced with permission.^[13a] Copyright 2013, Wiley-VCH. b) Schematic illustration of the fabricated asymmetry supercapacitor based on the wrinkled MnO_2/CNT hybrid film as a positive electrode and $\text{Fe}_2\text{O}_3/\text{CNT}$ hybrid film as a negative electrode. c) SEM image of the wrinkled MnO_2/CNT film. d) SEM image of the wrinkled $\text{Fe}_2\text{O}_3/\text{CNT}$ film. Reproduced with permission.^[68] Copyright 2016, The Royal Society of Chemistry. e) Photograph of a SWCNT stretchable solid-state micro-supercapacitor array based on serpentine design. f–g) Photographs of the micro-supercapacitor array connected to a LED upon bending and stretching, respectively. Reproduced with permission.^[73] Copyright 2013, American Chemical Society.

and even increased slightly, as the tensile strain increased up to 40%. Moreover, intrinsically stretchable nanomaterials such as ultrathin AuNWs could be stretched up to 50%, even without pre-strain of elastomeric substrates.^[51] The as-fabricated AuNWs membrane, with thickness of only 8 nm, was further used as highly transparent and stretchable electrodes for a wearable and invisible supercapacitor.^[51] The self-assembled AuNWs film exhibited a high transparency of $\approx 90\%$ at a wavelength of 550 nm. The resultant symmetrical supercapacitor could maintain a transparency of $\approx 80\%$ with reversible stretchability of 30% strain, without degradation over 80 stretching cycles.

Apart from the buckling configuration, the serpentine bridge–island design is also introduced for the fabrication of stretchable supercapacitors, especially for the integration of supercapacitors into a stretchable electronic circuit. In 2013, a stretchable micro-supercapacitor array with planar SWCNT electrodes and an ionic-liquid-based triblock copolymer electrolyte was reported.^[73] The narrow and long serpentine metallic interconnections were encapsulated with polyimide thin film to ensure that they were within the mechanical neutral plane

(Figure 8e). The metallic bridging interconnects will take most of the mechanical energy upon stretching, to protect the micro supercapacitor arrays from deformation. As a result, the formed micro-supercapacitor array showed excellent performances, which were stable over bending and stretching up to 30% without any noticeable degradation (Figure 8f,g). Furthermore, nine micro-supercapacitors could be easily integrated in a $1.5 \times 1 \text{ cm}^2$ pad, which could light up a micro-LED. Such CNT film could form composite with V_2O_5 nanowires to further improve the electrochemical capacitance.^[74] Supercapacitors based on this film showed a high volume capacitance of 80 F cm^{-3} at a scan rate of 10 mV s^{-1} and an excellent energy density of 6.8 mW h cm^{-3} , which is comparable to that of a lithium film battery ($1\text{--}10 \text{ mW h cm}^{-3}$).

3.1.3. 3D Textile/Porous-Based Configuration

A textile is an intrinsically flexible or even stretchable porous substrate weaved and/or knitted by yarns. An energy-storage system in a textile configuration is easy to be incorporated with

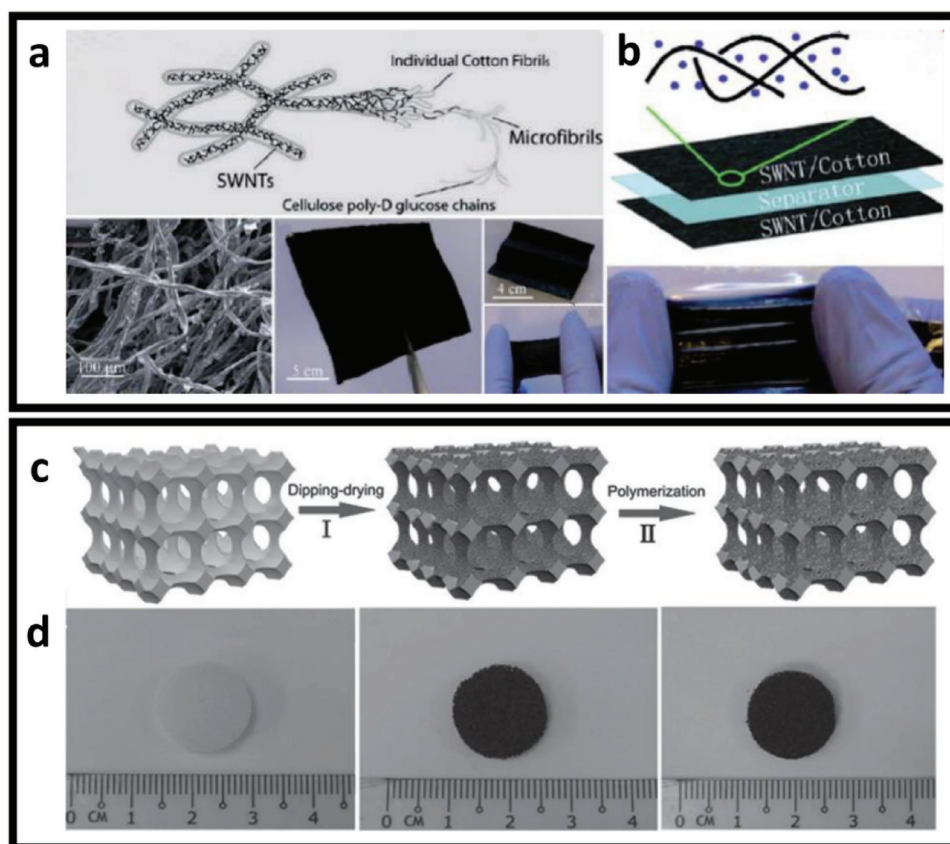


Figure 9. a) Scheme, SEM image and photographs of a textile stretchable electrode based on SWNTs. b) Scheme and photograph of a stretchable supercapacitor based on two stretchable textile electrode and a layer of electrolyte/seperator in between. Reproduced with permission.^[37] Copyright 2010, American Chemical Society. c) Scheme of the fabrication process of a porous compressive sponge electrode based on PANI-SWCNT composite. d) The corresponding photographs of the PANI-SWCNT sponge before and after dipping-drying and polymerization process. Reproduced with permission.^[78] Copyright 2015, Wiley-VCH.

everyday cloths, thus have attracted considerable attentions for powering wearable electronics.^[75] The high conductivity of textile electrodes could be achieved simply by a “dipping and drying” method with concentrated SWNTs ink.^[37] The conductive textiles showed good flexibility and had a strong adhesion between the SWNTs and the textiles (Figure 9a). In addition, the as-fabricated supercapacitors (Figure 9b) showed no obvious change in specific capacitance before and after stretching of 120% for more than 2000 cycles. More importantly, the 3D structure of the electrode can effectively increase the mass loading of active materials, benefiting from a much higher specific area compared with 2D film-based electrodes. Consequently, stretchable supercapacitors using these conductive textiles achieved a high areal capacitance of 0.48 F cm^{-2} , which could be even increased further to 24 folds by the loading of pseudocapacitive materials (MnO_2) into these conductive textiles. Stretchability of textile based on inelastic yarns mainly relied on the weaving structure. Another effective method, based on a textile structure alternately interwoven with inelastic and elastic yarns, showed an extended stretchability of up to 200% without significant conductivity decreases upon stretching.^[76] The textile could be formed by wounding elastic Spandex yarns around inelastic polyester yarn loops with a repeating zigzag pattern. The supercapacitors using this

textile coated with MWCNTs showed consistent capacitance of 35 F g^{-1} at 0.25 A g^{-1} , at different strains. The textile capacitors were also tested under dynamic and biaxial stretching modes, which showed good consistency of cyclic voltogramm profiles with 0–200% dynamic strain and 50% biaxial strain.

In addition, conductive polymers have been widely used for textile-based stretchable supercapacitors. An even coating of conductive polymer on textile surfaces could be achieved by technologies such as electrochemical polymerization,^[76] oxidative coupling polymerization,^[77] and in situ polymerization.^[39] An in situ polymerization of vacuum-deposited PEDOT-modified textiles was demonstrated for stretchable supercapacitor applications in 2016.^[39] The PEDOT-modified fabrics exhibit good flexibility, stretchability (up to 100%), and high conductivity. Fabric-based supercapacitors prepared via this method exhibit high areal (0.64 F cm^{-2}) and volumetric (5.12 F cm^{-3}) capacitance, as well as excellent cycling stability. The capacitance of the devices remained nearly unchanged even after 50000 cycles.

Sponge is another intrinsically stretchable and compressible porous substrate with high surface area. In 2016, A highly compressible all-solid-state supercapacitor based on PANI/SWCNTs/sponge electrodes was demonstrated.^[78] The PANI/SWCNTs/sponge electrodes were achieved by a

“dipping and drying” strategy to coat a SWCNT layer onto the skeleton of sponge, and a subsequent chemical oxidation polymerization process to prepare PANI on the surface of SWCNTs (Figure 9c,d). Based on PANI/SWCNTs/sponge electrodes, highly compressible all-solid-state supercapacitors were prepared using PVA/H₂SO₄ gel as the electrolyte. The performance of as-prepared supercapacitors remains nearly unchanged when being compressed with a 60% strain. More importantly, owing to the all-solid-state configuration, several supercapacitors can be integrated and interconnected together in series or parallel on one chip to improve the output potential and/or current.

3.2. Stretchable Batteries

The design of wearable and implantable biomedical devices systems, including data collection components, data transmission components, and data analysis components require a stretchable, lightweight, biocompatible, and continuous power-source device. Compared to supercapacitors, batteries showed a higher energy capacity, which is critical for long-term monitoring of human health, especially for implantable applications. To date, a handful of publications in the literature have demonstrated both stretchable primary batteries (e.g., alkaline batteries, dry batteries) and rechargeable batteries (mainly lithium-ion batteries). In the following section, the recent progress in stretchable batteries will be introduced, with the main focuses on the performances, stretching reliability, long-term stability, and biocompatibility of the devices, which are all key parameters for wearable biomedical applications.

3.2.1. Stretchable Lithium-Ion Batteries

Currently, lithium-ion batteries have dominated the battery market for a diverse range of applications, mainly due to their high energy capacity and light weight. As for stretchable LIBs, novel intrinsically stretchable materials such as carbon nanotubes or graphene have been attempted, but could hardly compete with the traditional active materials.^[79,80] Therefore, the current research directions to construct stretchable LIBs mainly concentrate on the structural design of conventional LiCoO₂ (LCO), LiMn₂O₄ (LMO), and Li₄Ti₅O₁₂ (LTO), or the composite of conventional materials with intrinsically stretchable materials.^[81] Similar to supercapacitors, structural design including wavy configuration, fibre configuration, porous/textile configurations, and serpentine bridge-island configurations have been applied for the fabrication of stretchable LIBs. In addition, novel origami/kirigami LIBs were also introduced to achieve significant deformability, especially with rigid electrode materials.

1D fibre-based LIBs can be easily woven into flexible textile, which had been proposed to represent an effective route to power skin-attachable biomedical devices.^[82] A novel, stretchable lithium-ion battery was designed by embracing LTO and LMO nanoparticles into two aligned MWCNT yarns that serve as the anode and cathode, respectively (Figure 10a).^[83] The wire-shaped battery typically exhibits an energy density of 27 W h kg⁻¹ or 17.7 mW h cm⁻³ and a power density of

880 W kg⁻¹ or 0.56 W cm⁻³. The flexible anode and cathode were further integrated into a spring structure to obtain a very elastic device. The capacity remained at 84% after the elastic battery had been stretched at a strain of 100% for 200 cycles. The merit for wire-shaped battery is that they could be woven into flexible textile and attached on normal cloths (Figure 10b,c), indicating its excellent compatibility with wearable electronic devices. Higher stretchability of up to 600% could be achieved by twisting similar electrodes onto an elastic fibre to work as the spring-structured, stretchable electrodes.^[82] However, the energy density of such a design is low because of the large volume of inactive elastic polymer substrates in the stretchable fibre battery. To address this problem, the same research group developed advanced spring-like fibre electrodes with an over-twisted, aligned MWCNTs and LMO/LTO composite.^[84] The resultant electrodes could be stretchable to larger than 300%, without using an elastomeric fibre as a core substrate, leading to an enhanced linear specific capacity of 600%. The battery based on springlike electrodes exhibited a stable performance, with a reduction of capacity of <1% after 300 stretching/releasing cycles at a strain of 50%.

Compared to fibre-shaped configuration, a porous scaffold has much higher surface area, thus showing great promise for the construction of LIBs with high electrochemical performance. However, traditional porous scaffolds for LIBs are rigid and not biocompatible, which is not a good choice for wearable and implantable biomedical application. To address this gap, PDMS has been used to fabricate porous and stretchable substrates for LIBs due to its beneficial properties, such as high mechanical stretchability, biocompatibility, and thermal stability.^[85] In 2012, a porous PDMS/CNT nanocomposite was first introduced for stretchable LIBs.^[86] In this study, a stretchable CNT/PDMS composite electrode as the anode for LIBs was prepared using porous PDMS obtained from the phase separation of poly(methyl methacrylate) (PMMA) in PDMS, and then extraction of PMMA. The porosity and stretchability of CNT/PDMS electrodes can be controlled by varying the ratio of PDMS/PMMA/block copolymer. The highest capacity per weight of active material was 190 mA h g⁻¹, which showed almost 670% larger capacity compared to the nonporous sample. However, this design could only achieve a low specific capacity (≈7 mA h g⁻¹), mainly due to insufficient penetration of Li-ions in the liquid electrolyte with CNTs in the pores. Also, the electrical performance of the battery was not assessed under stretching conditions. Further optimization of the pore structure is necessary to increase the capacity of the porous nanocomposites. In this case, PDMS sponge with an open network of pores has been applied for improving penetration of Li-ions in the electrolyte with electrodes. The 3D, porous, sponge-like PDMS scaffolds were fabricated via a sugar-cubes-templating strategy, where PDMS could be infiltrated into sugar-cube pores, and the sugar-cubes could be easily dissolved in water afterwards to form porous PDMS scaffolds.^[42] An electrode slurry consisting of active materials of the Li₄Ti₅O₁₂ (LTO) or LiFePO₄ (LFP) was then drop-casted on the PDMS sponge to serve as a stretchable anode and cathode, respectively. 82% and 91% capacity retention for the half cells using the stretchable LTO anode and LFP cathode could be obtained after 500 stretch-release cycles. A stable long-term cycle life of 70% capacity retention after

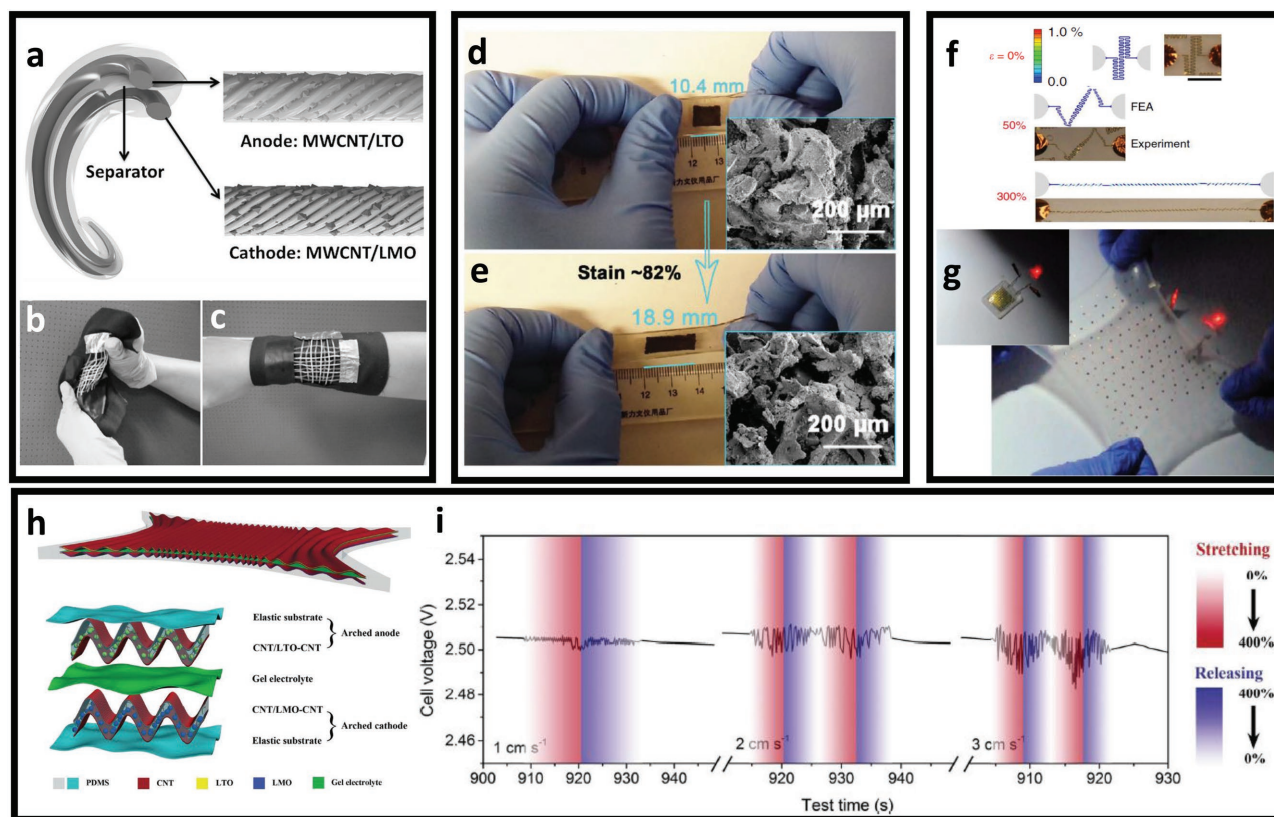


Figure 10. a–c) Scheme and photographs of a wire-like wearable LIBs. Reproduced with permission.^[83] Copyright 2014, Wiley-VCH. d,e) Photographs and SEM images (inset) of a 3D porous stretchable LIBs before (d) and after stretching (e). Reproduced with permission.^[42] Copyright 2016, Wiley-VCH. f) FEA and corresponding optical microscope images of a stretchable electrode based on self-similar serpentine design. g) Photographs of a stretchable LIB with an illuminated LED powered by this battery before (inset) and after biaxial stretching based on the fractal design. Reproduced with permission.^[27] Copyright 2013, Nature Publishing Group. h) Scheme of the structure of a wavy-based, superstretchy LIBs. i) Voltage profiles of the battery when discharging at 1C under stretching/releasing at increasing stretching/releasing speeds. Reproduced with permission.^[88] Copyright 2015, Wiley-VCH.

300 cycles was also observed in the stretchable full cell composed of the stretchable LTO anode and LFP cathode. The electrodes could effectively offer elastic response to large strain deformations up to 80% (Figure 10d,e). However, the battery showed a continuous decrease in performance with large strain, which is most likely due to an increase in resistance of the electrodes during stretching. In addition, graphene foam was also served as porous current collectors for flexible LIBs with robust cycle life and fast charge/discharge rate.^[87]

Maintaining stable performance of LIBs upon stretching is critical for wearable and implantable biomedical applications, as any disturbance in electricity output may result in signal interference with data collection component. Therefore, advanced structure design such as the serpentine bridge–island design is used for developing highly stretchable LIBs with traditional rigid electrode materials. In 2013, A set of design and manufacturing concepts for highly stretchable lithium-ion battery arrays has been proposed, based on a segmented design in the active materials and self-similar interconnect structures in between.^[27] The whole device was supported by a super-elastic silicone-rubber substrate, which offers a biaxial stretchability of 300% (Figure 10f,g), while maintaining capacity densities of $\approx 1.1 \text{ mA h cm}^{-2}$. At the same time, the surface coverages

of active materials could achieve as high as 50% by using the self-similar design, which makes full use of a limited space of bridging electrodes by increasing the fractal order.^[28] In addition, an integrated stretchable and wireless charging systems have been designed, fabricated, and integrated into the battery system. This feature is especially valuable for continuous powering of implantable devices, as the battery could be charged without establishing physical connections to external energy supplies. In addition, a wavy configuration has been used for the construction of stretchable LIBs recently.^[88] The battery consists of an arched anode, a gel electrolyte, and an arched cathode, which are finally packaged by an elastic polymer. The extension of the waves of the electrodes determines the stretchability of the battery (Figure 10h). Anode and cathode consist of random CNTs blended with LMO or LTO nanoparticles to create a conductive network, then the blend is inserted between the two CNT sheets, forming a sandwich structure. The wavy electrodes with the sandwich configuration demonstrated stretchability as high as 400% with almost unchanged capacity after 500 stretching cycles. More importantly, there was no noticeable increase in resistance of the electrodes during stretching, which enabled retaining the electrochemical performance of the LIBs upon dynamic stretching from 0% to

400% to 0%, with various stretching frequencies (Figure 10i). However, the electrodes with an areal active material loading density of $>6 \text{ mg cm}^{-2}$ exhibited large resistance changes upon stretching, which restrict further improvement in the energy density of the device.

Origami or kirigami design constitutes an additional strategy to fabricate LIBs with an unprecedented high level of deformation, without sacrificing surface coverages and loading of active materials.^[30,32,34b] Conventional planar LIBs consist of many layers, including current collectors, an anode and cathode, a separator, and packaging. The origami or kirigami LIBs were realized by folding these layers into desired specific patterns to enable their stretchabilities. For instance, an origami-LIB based on a Miura-ori pattern could allow a linear deformability of 1300% for a 45° Miura pattern with 5×5 parallelogram faces,^[30] provided by the folding and unfolding of the creases. To achieve good foldability and electrical conductivity at the creases after cyclic folding and unfolding, CNT was coated on active material layers of the origami paper as the current collectors. It is also possible to design kirigami-based LIBs with enhanced stretchability, which could be produced by standardized battery manufacturing.^[34b] It was shown that fracture due to cutting and folding was suppressed by plastic rolling, leading to stable electrochemical performances under mechanical deformations. Over 85% capacity retention and a Coulombic efficiency of 99.8% over 100 cycles could be achieved for the kirigami LIBs under compact and stretched states. Despite this, the overall origami- or kirigami-based LIB devices are too rigid and bulky to wearable or skin-attachable. Further endeavour need to be directed towards miniaturization of such devices with micro-metre-scale thickness so that they could be used in future wearable or implantable electronics.

3.2.2. Other Stretchable Batteries

Primary battery has been the most widely used energy storage devices since its invention in 1901. Nowadays, primary alkali manganese cells still represent a large share of portable battery market, mainly due to their extremely low cost and easy disposal.^[89] The first stretchable primary dry cell was reported in 2010.^[90] The concept for the ultra-compliant dry cells was based on the integration of highly elastic carbon-black silicone oil paste electrodes into a stretchable acrylic elastomer (VHB 4910 from 3M, introduced for dielectric elastomer actuators).^[91] Figure 11a illustrated the design of a stretchable cell consisting of the cathode made from zinc, carbon, and xanthan, and the printed anode made from manganese dioxide, carbon, and electrolyte (NH_4Cl , ZnCl_2) pastes. Based on this configuration, the stretchable dry gel cell could be stretched biaxially up to 100% (Figure 11b,c). Nevertheless, the discharge capacity decreased sharply from 7 mAh to 3.1 mA h when the battery was stretched up to 50%. This was likely caused by the delamination between the carbon-oil current collector and the electrodes. In 2014, a silver–zinc battery based on stretchable AgNWs and electroplated Zn electrodes was presented (Figure 11d,e).^[92] The fully stretchable batteries maintained their functions even when stretched to 80% (Figure 11f) and were stable over 1000 cycles. However, the energy density of this AgNW-Zn-based battery

($0.44 \text{ mW h cm}^{-2}$) was lower than conventional printed silver–zinc batteries (4 mW h cm^{-2})^[93] due to the much smaller active-layer thickness. Stretchable Mg batteries were also introduced based on electrodeposited polypyrrole (PPy) on buckled Au electrodes produced from the pre-stretching strategy.^[15] The electrodes were quite stable with less than one-fold resistance increase after being stretched to 30% for 2000 times. The battery was assembled using stretchable electrode PPy as cathode, Mg plate as anode, and phosphate buffered saline as electrolyte. This led to a durable cell with an operating voltage of 1.12 V after over 2000 times stretching at a strain of 30%. Recently, an all-printed stretchable Zn– Ag_2O battery was demonstrated by incorporating polystyrene-*block*-polyisoprene-*block*-polystyrene as a hyperelastic binder for custom-made printable inks (Figure 11g). The printed stretchable battery maintains a constant LED brightness regardless of severe torsional strain (Figure 11h–l). In addition, a reversible capacity density of $\approx 2.5 \text{ mA h cm}^{-2}$ is achieved after multiple iterations of 100% stretching.^[94]

Moreover, stretchable metal–air batteries, such as zinc–air batteries^[95] and aluminium–air batteries,^[96] have also been reported recently. In principle, a metal–air battery possesses a theoretical energy density much higher than that of the currently-dominant lithium-ion battery, which is promising for thin, skin-like energy devices for wearable and implantable electronics. For example, a stretchable and rechargeable fibre-shaped Zn–air battery was demonstrated by using aligned CNT sheets for the air cathode with a spring-like structure. The battery could be discharged/charged at 1V at a high current density of 1 A g^{-1} , showing the promise to power various miniaturized devices. As a demonstration, such designed batteries could be easily woven into textile for wearable electronics, such as a smart watch.

4. Stretchable Energy Conversion Devices

4.1. Stretchable Photovoltaic Devices

Solar energy is the most abundant renewable energy on the earth, as the earth receives more solar energy in an hour than the total energy it consumes in a year.^[97] Photovoltaic devices have the potential to produce substantial amount of power to meet the typical power consumption of most biomedical devices.^[98] However, the use of photovoltaic devices for wearable biomedical applications is limited by 1) the availability and the intensity of the light sources; 2) the rigid nature of the photovoltaic materials; and 3) the availability of body surface-area for attaching photovoltaic devices. Despite the challenges above, several photovoltaic technologies have been developed in ultraflexible or stretchable form factors while still providing decent energy densities.^[3f] We will here discuss viable technologies in stretchable and wearable photovoltaic devices suitable for wearable and implantable biomedical applications.

4.1.1. Stretchable Photovoltaic Devices from Inorganic Materials

The current solar cell industry is dominated by inorganic solar cells, especially Si based solar cells,^[97b,99] mainly due to the high

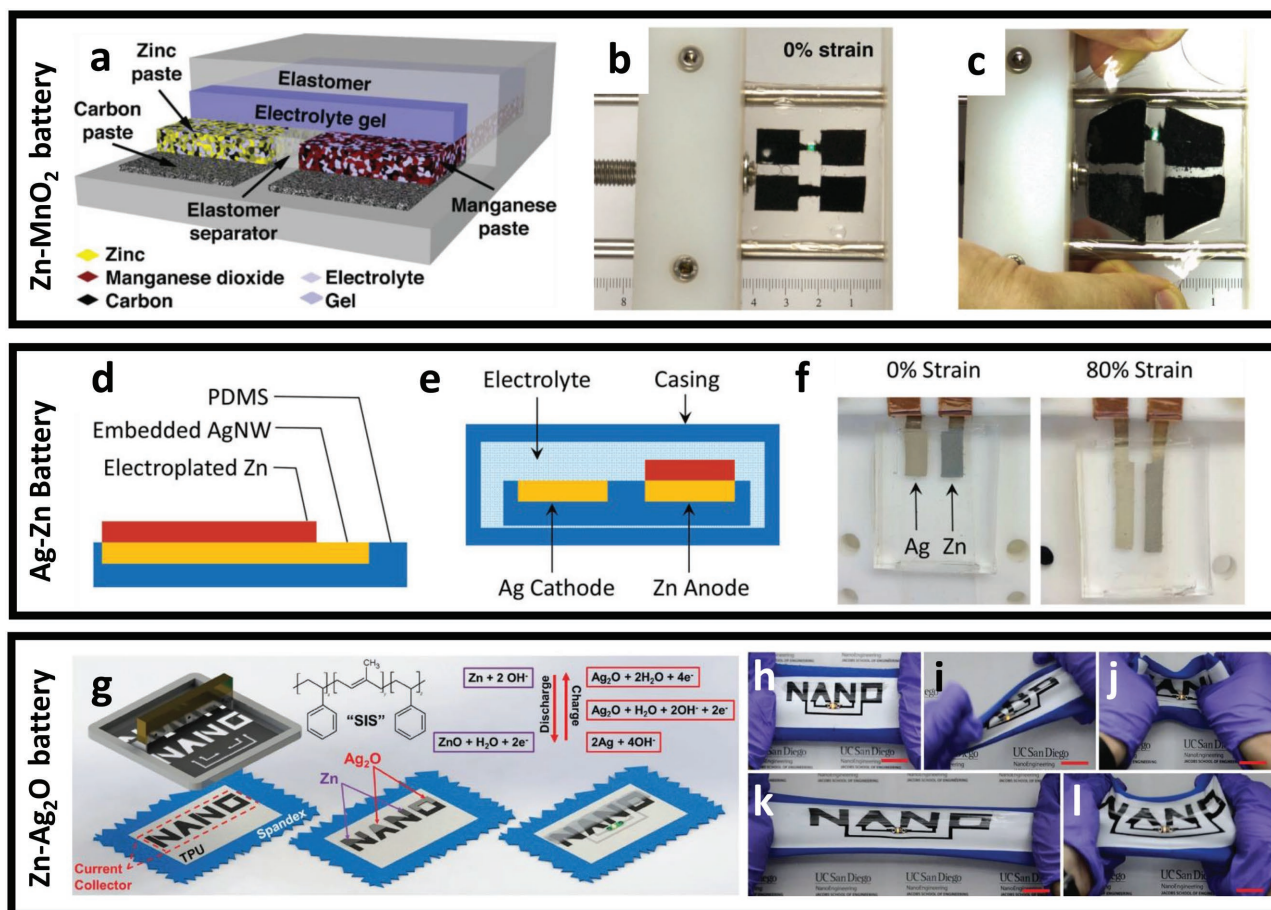


Figure 11. a) Scheme of the structure of a stretchable Zn-MnO₂ battery. b,c) Photographs of the stretchable battery at strain of 0% (b) and with biaxial stretching (c). Reproduced with permission.^[90] Copyright 2010, Wiley-VCH. d,e) Cross-sectional schemes of a stretchable Zn electrode (d) and full battery (e), respectively. Metallic Zn microstructures were deposited onto the stretchable AgNW electrodes via electroplating. f) Photographs of the stretchable full battery at 0% and 80% strain. Reproduced with permission.^[92] Copyright 2014, Wiley-VCH. g) Screen-printing steps of a Zn-Ag₂O battery on a stretchable textile using a SIS binder. Inset: Redox charge and discharge reaction. h-l) Photographs of sealed battery while being 0% stretched (h), twisted (i), indentation strains (j), 100% stretched (k), and biaxial stretched (l). Scale bar: 2.25 cm. g-l) Reproduced with permission.^[94] Copyright 2017, Wiley-VCH.

energy-conversion efficiency and reliability of this type of photovoltaic material. Such a type of solar cells is intrinsically brittle and fragile with limited stretchability. Nevertheless, high stretchability could be achieved with the STS strategy, with buckled or serpentine design. In 2006, a single-crystal Si thin-film was processed into periodic wave-like geometries enabling reasonably high stretchability.^[6] The p-n-junction photodiode following this configuration could be compressed and stretched. The photovoltaic performance was largely retained when under cyclic compressing (up to ≈5% strain) and stretching (up to ≈15% strain) for over 100 times. Later in the same year, wavy GaAs and Si nanoribbons were reported to form on elastomer surfaces (Figure 12a).^[11] The buckling geometries could be well-controlled with extended stretchability (up to 100%), compressibility (up to 25%), and bendability (curvature radius down to 5 mm). Interestingly, the photovoltaic performance of the device was found to be improved when the nanoribbon electrode was stretched up to 44.4% (Figure 12b), which was attributed to the increased effective area when the buckled ribbon was stretched. Following this kind of concept, a stretchable GaAs photovoltaic system was demonstrated using the aforementioned bridge-island configuration.

Stretchability was realized by localizing strain at the interconnect position and away from the active devices.^[100] The resulted configuration enables high areal coverages of ≈70%. As a result, energy conversion efficiency and fill factors can reach to ≈13% and 0.79, respectively, which are both constant after more than 500 cycles of biaxial stretching (20%). With further optimization of the interconnect-island geometry, a natural form of strain-limiting behavior was observed.^[101] The whole devices could endure 60% of biaxial stretching, due to the use of curved interconnections. The energy conversion efficiency and fill factors are further improved to 19% and 0.85, respectively. Further attempts for inorganic stretchable solar cells were attributed to the transfer printing process of inorganic amorphous thin film semiconductors to elastomeric substrates. In 2016, a water-soluble germanium oxide sacrificial layer was developed to transfer amorphous Si thin-film solar cells to PDMS substrates with serpentine designed electrodes.^[102] Figure 12c-h shows optical micrographs of the solar cell arrays with tensile strains ranging from 0–50%. The current-voltage characteristics (Figure 12i), energy conversion efficiency, and fill factors (Figure 12j) of the stretchable solar cell does not decrease even after stretching to 50%.^[102]

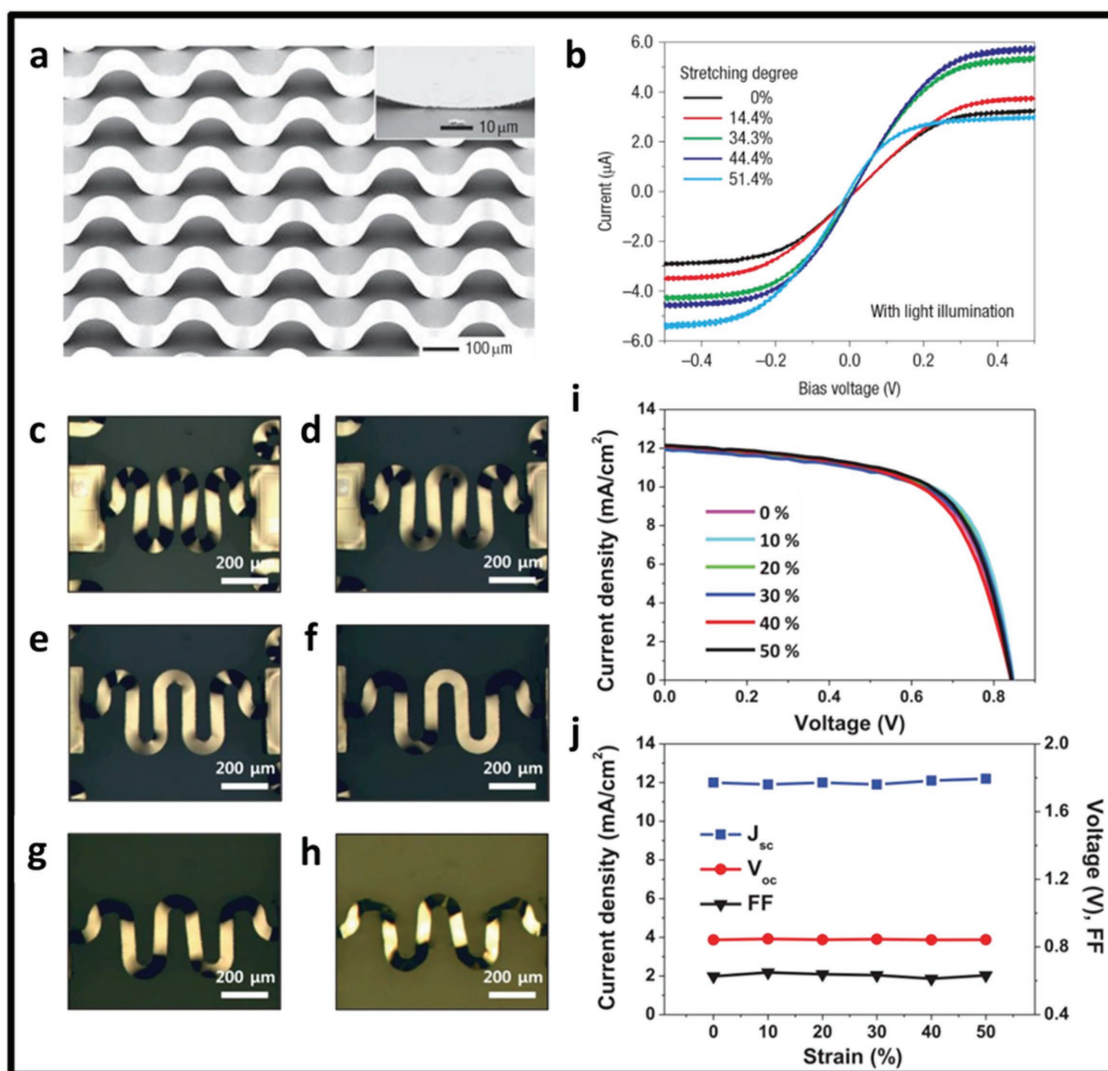


Figure 12. a) Stretchable, wavy silicon ribbons and b) I - V characteristics of photovoltaic devices illuminated with constant luminance and stretched to different degrees. Reproduced with permission.^[11] Copyright 2006, Nature Publishing Group. c-h) Optical images of amorphous Si solar cell interconnected by serpentine bridges under applied strain of 0% (c), 10% (d), 20% (e), 30% (f), 40% (g), and 50% (h). i) Current-density-voltage characteristics of stretchable amorphous Si solar cells as function of applied strain. j) Representative photovoltaic parameters of stretchable amorphous Si solar cells as function of applied strain. Reproduced with permission.^[102] Copyright 2016, Wiley-VCH.

4.1.2. Stretchable Photovoltaic Devices from Organic Materials

Compared with inorganic photovoltaic devices, organic photovoltaics are typically much thinner, giving rise to high flexibility of the overall devices to enable conformal contact with human skin.^[3f,103] In 2011, the first stretchable organic photovoltaic device was demonstrated by using PEDOT:PSS with poly(3-hexylthiophene):phenyl-C61-butyric acid methyl ester (P3HT:PCBM) film on pre-strained PDMS substrate.^[53b] The film was with buckled structures using pre-strain techniques. The short circuit current and the open circuit voltage slightly increased with strain applied. However, the fill factor (0.38) and efficiency (1.2%) of the device were still far behind those for stretchable inorganic counterparts.^[100,101] In another design, an ultrathin and lightweight organic solar cell was obtained, showing excellent mechanical compliance.^[104] By depositing

P3HT:PCBM on a PEDOT:PSS electrode with thin PET film as the substrates, the overall thickness of the device was just 1.9 μm (Figure 13a). The current solar cell holds the current record for specific power of organic solar cells (10 W g⁻¹) and can function with a bending radius of 35 μm. Furthermore, after adhering the flexible organic solar cell to a pre-strained VHB elastomer, the device could afford compression to 70% and tensile strain to 400%, while remaining functional (Figure 13b). The cyclic compression showed a gradual decrease in the short circuit current (I_{sc}), the fill factor, and the output power, resulting in a 27% decrease in power after 22 cycles. In spite of this, the configuration still represents state of the art stretchable organic solar cell with over 4% power conversion efficiency. To further extend the flexibility and power conversion efficiency of solar cells, all-polymer solar cells (all-PSCs) consisting of polymer-donor and polymer-acceptor materials have been introduced

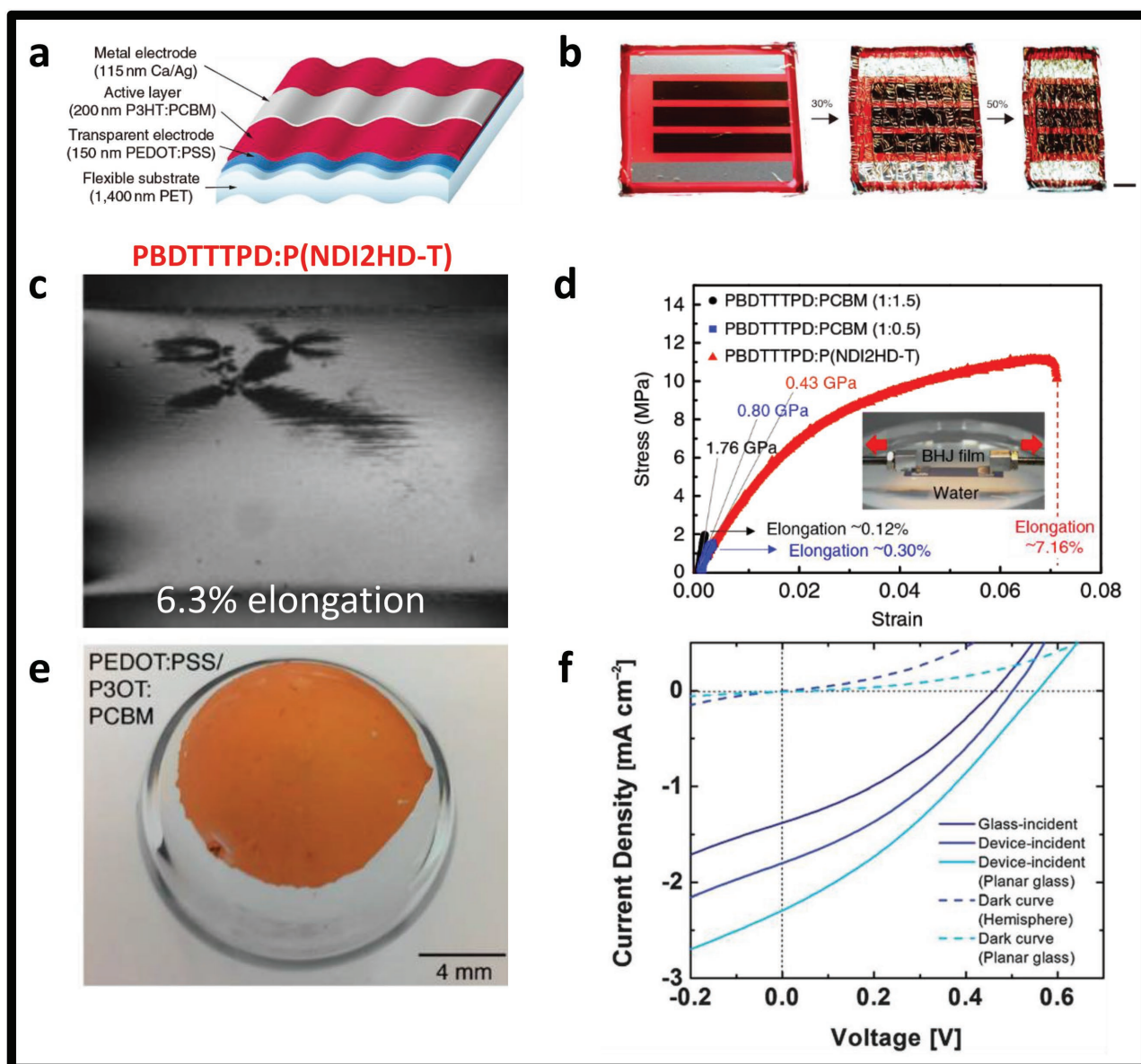


Figure 13. a) Scheme of a stretchable organic photovoltaic cells. b) Stretchable solar cells made by attaching the ultrathin solar cell to a pre-stretched elastomer. They are shown flat (left) and at 30% (middle) and 50% (right) quasi-linear compression. Scale bar: 2 mm. Reproduced with permission.^[104] Copyright 2012, Nature Publishing Group. c) Optical microscope images of PBDTTTPD:P(NDI2HD-T) (1.3:1 w/w) blend films when the film were under different strains. d) Strain–stress curves of PBDTTTPD:PCBM and PBDTTTPD:P(NDI2HD-T) blend films. Reproduced with permission.^[105] Copyright 2015, Nature Publishing Group. e) Photographs of bilayer film comprising PEDOT:PSS/P3HT:PCBM (left) and PEDOT:PSS/P3OT:PCBM (right) on the hemispherical glass surfaces. f) Current density vs voltage for an all-organic PEDOT:PSS/P3HT:PCBM solar cell onto both hemispherical and planar glass surface. Reproduced with permission.^[106] Copyright 2014, The Royal Society of Chemistry.

to replace polymer–fullerene solar cells. In 2015, an all-PSC was fabricated using poly[4,8-bis(5-(2-ethylhexyl)thiophen-2-yl)-benzo[1,2-b:4,5-b']dithiophene-*alt*-1,3-bis(thiophen-2-yl)-5-(2-hexyldecyl)-4H-thieno[3,4-c]pyrrole-4,6(5H)-dione] (PBDTTTPD) as the electron donor, and poly[[N,N0-bis(2-hexyldecyl)-naphthalene-1,4,5,8-bis(dicarboximide)-2,6-diyl]-*alt*-5,5'thiophene] (P(NDI2HD-T)) as the electron acceptor.^[105] The flexible solar cell exhibited higher power-conversion efficiency of 6.64% than the control polymer–fullerene devices with PCBM as the electron acceptor (6.12%). Moreover, The intrinsic mechanical properties

of the PBDTTTPD:P(NDI2HD-T) without substrates were measured. As indicated in Figure 13c,d, the tensile modulus of the PBDTTTPD:P(NDI2HD-T) blend film was only 0.43 GPa, and its elongation at break of the blend was 7.16%, which was a 60-fold enhancement over that of PBDTTTPD:PCBM.^[105]

Recently, an ultraflexible thin-film organic solar was introduced with the ability of being conformally bonded to hemispherical surfaces with radii of only 8 mm.^[106] Instead of using P3HT as the active material, poly(3-octylthiophene) (P3OT) was chosen due to its much better mechanical

compliance with hemispherical surfaces. The elasticity of regioregular polythiophenes increases by a factor of seven with an increase in the length of the alkyl pendant groups, from hexyl to octyl, with a corresponding increase in ductility. As a result, the compliant PEDOT:PSS/P3OT:PCBM thin film exhibited no observed wrinkling or cracking after transferred to hemispherical glass surfaces (Figure 13e), which equals to a biaxial tensile strain of 24%. In comparison, PEDOT:PSS/P3HT:PCBM thin film showed extensive cracking after being transferred to hemispherical glass surfaces. The all-organic device exhibited a reduction in open-circuit voltage with an increase in short-circuit current density by approximately 27% (Figure 13f). Nevertheless, the efficiency of P3OT:PCBM-based solar cells is estimated to be only $\approx 0.36\%$, which is mainly due to inferior charge-transport properties of P3OT, whose hole mobility in field-effect transistors is ten to fifty times lower than that of P3HT. Further studies found that poly(3-heptylthiophene) (P3HpT) and PCBM have mechanical properties similar to that of P3OT, and electronic properties comparable to P3HT,^[107] which makes it attractive as a potential replacement for P3HT in stretchable, wearable, and mechanically robust solar cells. Consequently, an ultraflexible organic solar cell based on P3HpT:PCBM was demonstrated in 2016.^[108] This ultraflexible device could be conformally attached to the human body and generated stable power supplies under repeating (≈ 1000 cycles) compressive strain of 75% and a tensile strain of 5%. The power density of the resultant devices is $\approx 1 \text{ mW cm}^{-2}$ under natural sunlight (98 mW cm^{-2}) and $\approx 10 \text{ }\mu\text{W cm}^{-2}$ under diffuse artificial light.^[108]

4.1.3. Stretchable Wire-Shaped Photovoltaic Devices

Another example of transforming rigid materials into stretchable devices was introduced with wire-shaped configuration. Dye-sensitized solar cells were fabricated in a spring-like architecture to accommodate 30% uniaxial strain (Figure 14a–d). The solar cell consisted of two stretchable fibre electrodes (a rubber fibre wrapped with conductive CNT sheets and a modified active titanium wire), both of which were encapsulated by transparent polyethylene tubes (Figure 14a). The device was completed by filling the cavity of the tube with a liquid redox electrolyte and sealing the device.^[109] A single cell of the wire-like solar harvester exhibited power conversion efficiency of 7.13% in its natural state. The J - V curves of a solar cell wire cell before and after stretching by 30% for 20 cycles was presented in Figure 14e, where J_{SC} only decreased slightly by 3%, possibly due to the peeling off of a few of TiO_2 nanotubes. Multiple devices could be assembled into a stretchable “photovoltaic textile” comprising five cells connected in series and parallel. This assembly retained $\approx 90\%$ of its original efficiency when subjected to 50 cycles of 20% strain (Figure 14f). Wearable fibre-shaped configurations have also been used to fabricate polymer solar cells and perovskite solar cells. For instance, an aligned CNT fibre and aligned TiO_2 -nanotube-modified Ti wire as two electrodes were twisted into a fibre-shaped polymer solar cell that showed a power conversion efficiency of 1.8%.^[110] Moreover, a recent attempt was successfully made to fabricate a perovskite solar cell by using CNT sheets as the transparent electrode and aligned TiO_2 nanotubes as the electron transporting layer with a coaxial structure.^[111] This perovskite solar

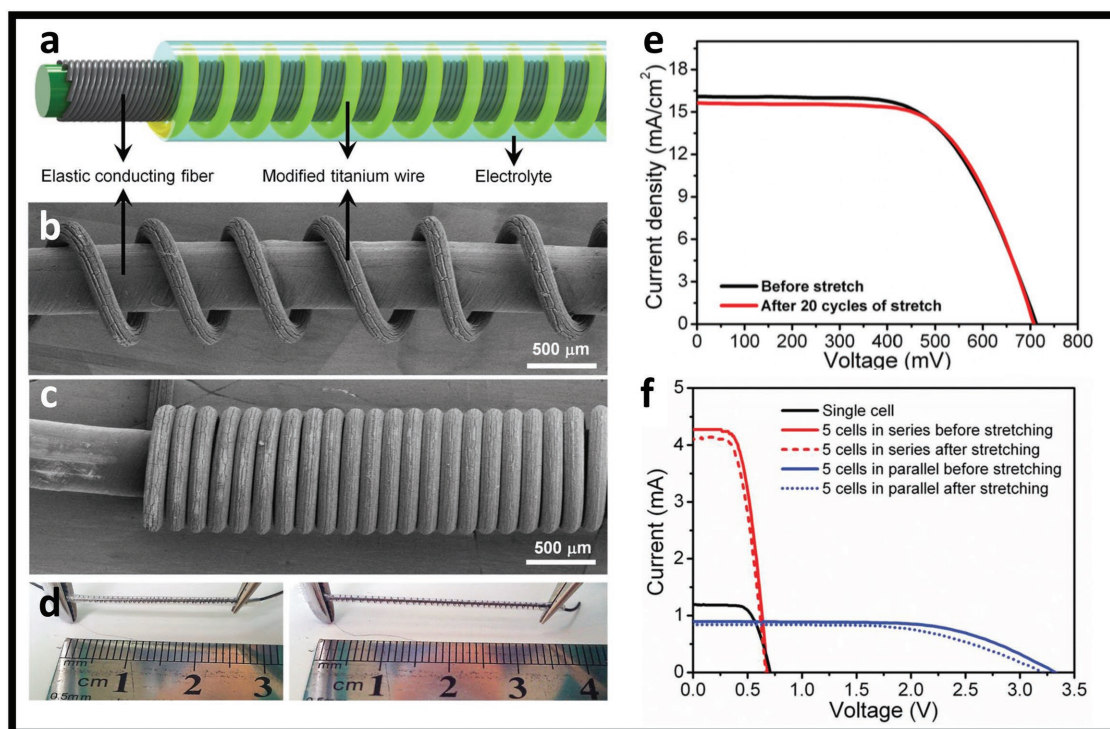


Figure 14. a) Scheme of a wire-shaped stretchable solar cell. b–c) SEM images of the solar cell before (bottom) and after (top) stretching. d) Photograph of the solar cell before (left) and after (right) stretching. e) J - V curves of a stretchable DSC before and after stretch for 20 cycles at a strain of 30%. f) J - V curves of the photovoltaic textile in series and parallel before and after stretch. Reproduced with permission.^[109] Copyright 2014, Wiley-VCH.

cell displayed a power conversion efficiency of 3.5%. In addition, other strategies like brush-printing CNTs-based^[112] or textile-based^[113] solar cells have recently attracted increasing attention due to facile large-scale fabrication.

4.2. Stretchable Generators

Harvesting energy from the human body could be an ultimate energy solution for self-sustainable wearable and implantable electronics.^[114] In particular, energy generated from biomechanical motions of the human body holds great promise to power on-body devices, such as wearable pressure sensors or implantable pacemakers. However, current energy-generation devices are made of rigid or brittle ceramic materials,^[115] which are neither stretchable to accommodate human motions, nor to enable conformal contact with human skin and/or tissues. This challenge can be, in principle, overcome by MTS or STS strategy. Typically, mechanical energy (such as heart beats,^[116] blood flow,^[117] walking,^[118] breathing,^[119] and stretching of muscles)^[120] and body heat are two main energy sources for electricity generation.^[120] To date, stretchable electricity generators can be categorized into three types: stretchable piezoelectric generators, stretchable triboelectric generators, and wearable thermoelectric generators. The first two types transform biomechanical energy into electricity, while thermoelectric generators convert body heat into electricity.

4.2.1. Stretchable Piezoelectric Generators

Piezoelectric materials generate electricity when they are mechanically deformed. Although the electrical energy supplied by a piezoelectric generator may be intermittent, a continuous energy supply is possible when it is coupled with an energy storage device.^[120] Hence, piezoelectric devices can be used to extend the lifetime of implantable devices. Highly sensitive piezoelectric devices can even directly transduce physical stimuli into electrical signals, making it possible to achieve self-powered sensors.^[121] Most high-performance piezoelectric materials are brittle inorganic materials with high-tensile moduli.^[122] For example, lead zirconate titanate (PZT, $\text{Pb}[\text{Zr}_{0.52}\text{Ti}_{0.48}]\text{O}_3$) has a piezoelectric coefficient ≈ 10 times higher than that for polyvinylidene fluoride (PVDF).^[123] However, PZT has an elastic modulus of 50–100 GPa,^[124] leading to materials fracture even under a tensile strain of 0.2%.^[125] In 2011, non-coplanar PZT nanoribbons were patterned into wave-like structures, allowing for flexing and stretching operating modes by transferring the mechanical strain to the amplitudes and wavelength of the buckled structures (**Figure 15a,b**).^[122] The buckled PZT nanoribbons exhibited a nearly two orders of magnitude increase in maximum tensile strain ($\approx 8\%$) without failure over their non-buckled counterparts ($\approx 0.1\%$). Moreover, the structures also exhibited an enhanced electromechanical performance attributed to a flexoelectric contribution to the piezoelectric coefficient, leading to a peak power density of 2.5 W cm^{-3} under uniaxial deformation.

Another viable and straight forward method is to integrate traditional piezoelectric materials with highly stretchable

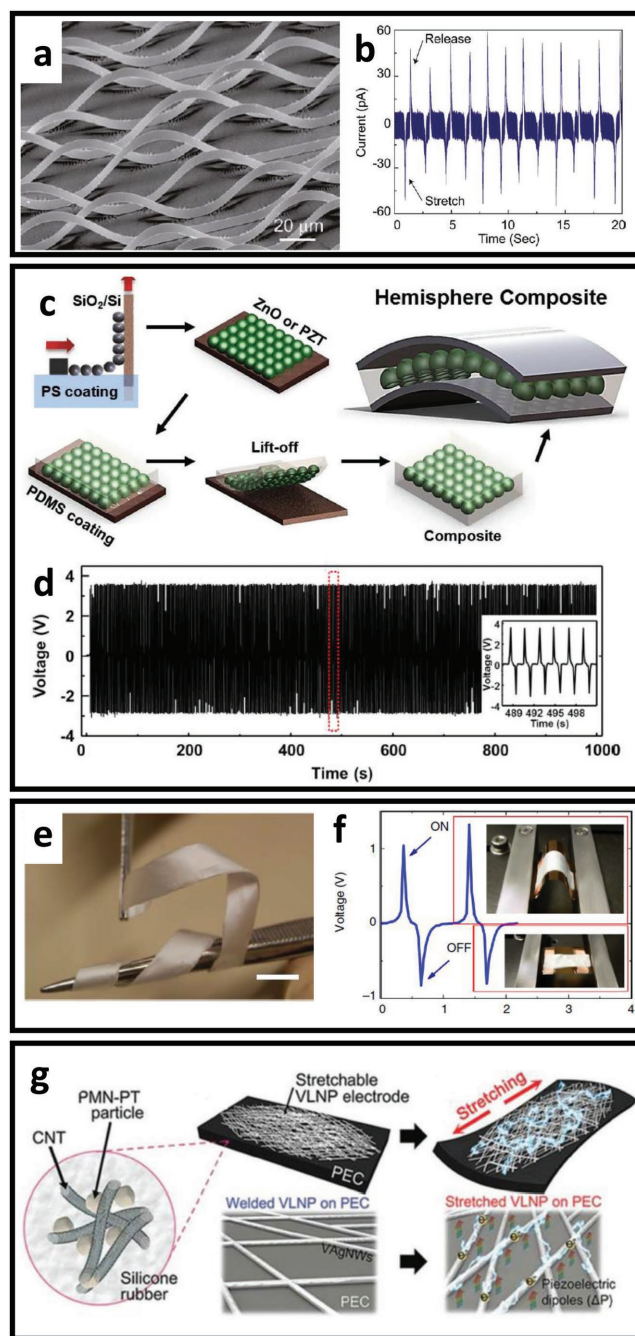


Figure 15. a) SEM image of a buckled PZT nanoribbon film. b) Short-circuit current measured from devices consisting of 10 ribbons under periodic stretch (8% strain) and release. Reproduced with permission.^[122] Copyright 2011, American Chemical Society. c) Schematic diagrams of the fabrication process for the piezoelectric hemispheres-embedded stretchable composites. d) The stability and durability test of 10-mm diameter ZnO hemispheres embedded composites. Reproduced with permission.^[126] Copyright 2014, Elsevier Ltd. e) Photograph of free-standing film of highly flexible P(VDF-TrFe) fibres. f) Measured voltage response of an array of P(VDF-TrFe) fibres under cycling bending at 1 Hz. The top and bottom insets show photographs of the device during bending and release, respectively. Reproduced with permission.^[121] Copyright 2013, Nature Publishing Group. g) Schematic illustration of the hyper-stretchable and deformable nanocomposite generator (left) and the final SEG device stretched by human hands (right). Reproduced with permission.^[128] Copyright 2015, Wiley-VCH.

materials for improved flexibility. Highly ordered piezoelectric hemispheres could be embedded into PDMS matrices, leading to stretchable energy harvesters,^[126] as illustrated in Figure 15c. Polystyrene (PS) beads were deposited on SiO₂/Si substrate to form the array as the templates, which was followed by sputtering of 100-nm-thick ZnO or PZT film on top of PS beads. PS templates were then burnt out by heating to form a hollow hemispheres structure on the surface of substrates, which was embedded into PDMS substrates to form a free-standing piezoelectric film. The nanogenerators with a single hemisphere layer generated an output voltage of up to 4 V at a current density of 0.13 $\mu\text{A cm}^{-2}$ (Figure 15d), which were increased up to 6 V and 0.2 $\mu\text{A cm}^{-2}$ by stacking three layers of such hemispheres layer-by-layer.^[126]

As discussed above, one-dimensional nanostructures (such as metallic nanowires) could sustain much higher tensile strain ($\approx 10\%$) before failure over their bulky counterparts ($< 1\%$). Similarly, one-dimensional polymer-based piezoelectric materials have been used as effective building blocks for fabrication of stretchable piezoelectric devices.^[127] The 1D structure was fabricated by electrospinning PVDF solution into fibres and then subjecting to pre-strained PDMS substrates. The resultant energy harvesters exhibited a high stretchability of 110%, which could generate current and voltage of ≈ 1.2 nA and ≈ 40 mV under periodic stretch and release of 30% strain at frequency of 0.5 Hz. Higher output could be obtained by increasing the applied strain, loading frequency and the number of fibres. However, energy harvested from single fibre was still too low to power wearable or implantable electronics. Therefore, large area and highly aligned polyvinylidene fluoride-trifluoroethylene (P(VDF-TrFe)) nanofibers were introduced through a modified electrospinning process.^[121] The aligned nanofibers can be formed into flexible, free-standing sheets, by use of electrospinning onto a fast rotating collector. The resulting materials are mechanically robust and can be handled easily, with the capability to be bent or twisted without fracture (Figure 15e). Under bending conditions, these fibres exhibit currents up to 40 nA and a voltage of about 1.5 V (Figure 15f). In addition, Mechanical-properties tests revealed that the P(VDF-TrFe) fibre arrays exhibited high stretchability by demonstrating maximum elongation of $\approx 100\%$ and elastic limit at $\approx 20\%$ strain. Furthermore, the P(VDF-TrFe) fibre arrays show excellent sensitivity in the low-pressure regime, which could also be applied as pressure sensors to measure both compressive and bending pressure as small as 0.1 Pa.

Hyper-stretchability in energy harvesters could be realized when the stretchability of all the energy-harvesting active materials, substrate, and electrodes were enabled.^[128] This stretchable energy harvester exhibits over ten times larger stretchability ($\approx 200\%$) and about seven times higher power output (≈ 4 V and ≈ 500 nA), compared to the previous stretchable piezo-nanogenerator. The outstanding performance was achieved by employing a rubber-based piezoelectric elastic composite and the very long nanowire percolation electrodes. The composite consisting of well-dispersed lead-magnesium-niobate-lead-titanate (PMN-PT) microparticles and CNTs embedded into an Ecoflex matrix (Figure 15g). The remarkable elastic responses of the composite to the large strain guaranteed a high degree of piezoelectricity, thus resulting in high-performance

energy harvesting. In addition, the high electrical conductivity of the silver nanowire percolation network was not significantly reduced after being stretched up to 200%, demonstrating notable stability under large elongation.^[128] Meanwhile, the stretchable piezoelectric nanogenerator exhibited a consistent voltage output with negligible degradation after 15000 cycles of stretching tests.

4.2.2. Stretchable Triboelectric Generators

Energy harvesting through the triboelectric principle has gained increased attention since the invention of the first triboelectric generator in 2012.^[129] The energy-harvesting principle of triboelectric nanogenerators (TEG) is based on the coupling of the triboelectric effect and electrostatic induction, where electrostatic charges created by physical contact of two dissimilar materials can generate a potential drop when the two surfaces are separated by a mechanical force.^[130] The output of triboelectric nanogenerators is highly dependent on the discrepancy of electron-attracting abilities of contacted surfaces, as there will be net negative charges on the surface with a strong electron-attracting ability and net positive charges on the surface with weak electron-attracting ability.^[14] The challenge of fabricating high-performance stretchable TENGs mainly lies at material choices, device layouts, and the integration with other electronic devices. Similar with piezoelectric devices, stretchable TENGs could be used as mechanical energy harvesters or self-powered sensors from the human body. PDMS can act as an excellent stretchable triboelectric layer interfacing with the human body, due to its highly stretchable and bio-compatible features. In 2014, a multifunctional, stretchable energy-harvesting electronic skin was demonstrated based on PDMS and SWCNT.^[131] The device consisted of layers of PDMS/SWCNT-film/porous-PDMS/PDMS-spacer/SWCNT-film/PDMS, as shown in Figure 16a. The porous PDMS surface was initially negatively charged and the surface charges were additionally generated and maintained through contact with the bottom SWCNT electrode via the triboelectric effect. The voltage generation using a finger tapping with an approximate pressure of 2 kPa is shown in Figure 16b. Moreover, the multilayer device with two different output signals (resistance and capacitance) is capable of detecting various mechanical stimuli, including bending, twisting, and lateral stretching with voltage and current generation in the range of tens of volts and tenths to several $\mu\text{A cm}^{-2}$, respectively. Consequently, instantaneous power on the order of several to tens of $\mu\text{W cm}^{-2}$ was generated. The energy-harvesting functionality can potentially be utilized to operate an e-skin device itself, as well as powering wearable health-monitoring sensors, such as temperature sensors, electrocardiogram sensors, and blood-pressure sensors.

In addition, the integration of triboelectric nanogenerators with other wearable components is addressed with a self-power platform consisting of a triboelectric nanogenerator, a supercapacitor, and a strain sensors.^[132] The stretchable electrode for all three devices is constructed with a AgNW/PEDOT:PSS/polyurethane composite (Figure 16c–e). The low power consumption allowed the strain sensors to be driven by a supercapacitor, which was charged using a triboelectric nanogenerator

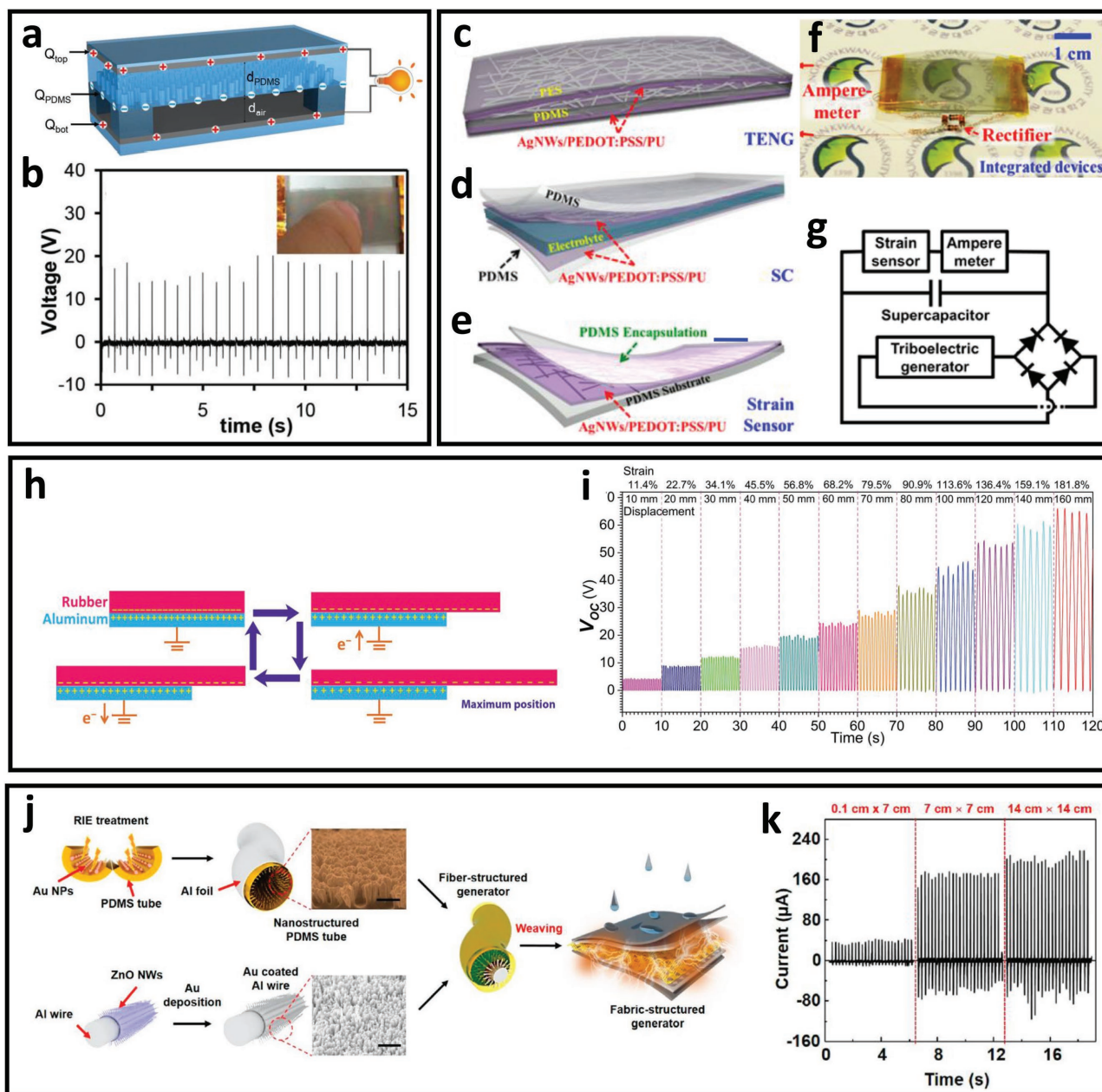


Figure 16. a) Schematic illustration of energy-harvesting mechanism of a stretchable energy-harvesting tactile electronic skin. b) Voltage generation by finger tapping with a pressure of 2 kPa. Reproduced with permission.^[131] Copyright 2014, Wiley-VCH. c–e) Schematic illustrations of individual components based on AgNWs/PEDOT:PSS/PU: c) stretchable TENG, d) stretchable supercapacitors, and e) stretchable strain sensor. f) Photograph of the integrated device. g) Circuit diagram of strain according to the sensor with supercapacitor charged by TENG. Reproduced with permission.^[132] Copyright 2015, American Chemical Society. h) Schematic illustration of the working principle of a rubber-based stretchable TENG. i) The measured output voltage under different stretched displacement/strains. Reproduced with permission.^[133] Copyright 2015, Wiley-VCH. j) Schematic diagrams of fabrication of a stretchable textile based TENG. k) Output current of the TENG with the active area. Reproduced with permission.^[135] Copyright 2015, American Chemical Society.

with PDMS and poly(ether sulfone) (PES) as active materials (Figure 16f,g). The TENG generated an output voltage of ≈ 40 V when subjected to a stretching strain of 10%. The detection of human activities (breathing, coughing, drinking, swallowing, and eating) that induce small strains and body motions that cause large strains were demonstrated using the integrated system.^[132]

Triboelectric nanogenerators based on the vertical contact–separation of top and bottom surfaces is not responsive to horizontal tensile strain. To address this challenge, a new type of stretchable TENG based on triboelectrification and electrostatic induction between a piece of stretchable rubber and an aluminium film was introduced.^[133] Upon repeated stretching and releasing of rubber, the single-electrode TENG

exhibited in-plane charge separation and results in a potential difference between the aluminium electrode and the ground. The schematic illustration of the working principle is shown in Figure 16h. The voltage output and the transferred charge density both increased upon increased stretch ratio (Figure 16i). Maximum power density ($\approx 76.27 \mu\text{W m}^{-2}$) of the TENG was achieved at a resistance of $\approx 2 \text{ G}\Omega$. The stretchability of the device was defined by the rubber layer, which could be stretched to $>180\%$ strain. Consequently, the stretchable could be mounted onto human body, and a self-powered health monitoring system could be realized for detections of physiological activities and joint movements.^[133] Another design of stretchable TENG was presented by assembling serpentine-patterned electrodes and a wavy-structured Kapton film.^[134] Owing to the unique structural design, the FTENG could be operated at both compressive and stretching mode, with an maximum open-circuit voltage of 700 V and a short-circuit current of 75 μA , corresponding to an instantaneous output power density of 5 W m^{-2} . The wavy structure of the Kapton film greatly enhanced the triboelectric output by providing sufficient distance for charge separation and the resultant potential difference for driving external circuit. Benefiting from advanced structural designs, the TENGs could withstand a tensile strain of up to 22% with strong shape adaptability and biocompatibility, which could be conveniently attached onto human body for self-powered body-motion sensing and mechanical-energy harvesting.^[134]

Textile design was an effective approach for enhanced stretchability, which could be used for TENG systems as well.^[135] The fiber-based coaxial structure is mainly consisted of Al wires and PDMS shells. Then ZnO nanowires were grown on the Al wire, followed by the deposition of a gold thin film acting as one electrode. The core of the PDMS tube was etched away, forming nanowire arrays with a length of 1–2 μm inside the tube. The Au/Al wires were inserted into the PDMS tube, and the resultant fibre was wrapped around by flexible Al thin film, which functioned as the other electrode (Figure 16j). The fibre-structured nanogenerator showed an output power of 40 V and 10 μA , with a stable output performance even under a high humidity environment condition. The FTENG was then fabricated by weaving the fibres, followed by bonding to a waterproof fabric for all-weather use. It showed a high output voltage and current value of 40 V and 210 μA , respectively, corresponding to an instantaneous power output of 4 mW under the same cycled compressive force (Figure 16k). The fabric was also found to be quite stretchable up to over 25%. Although the output current decreases by about 47.6% from 210 to 110 μA at this stage, the fabric can almost perfectly recover its original shape after release of the tensile force.

4.2.3. Wearable Thermoelectric Generators

Thermoelectric generators (TEGs) are devices that can produce electrical power from a temperature gradient. Unlike piezoelectric and triboelectric devices, TEGs offer continuous and stable power. However, the small temperature gradients of human body and loss of latent heat through evaporation of sweat limited the total power that could be converted by wearable thermoelectric generators.^[2,118] The efficiency of

thermoelectric conversion is largely determined by the active materials. Semiconductor materials are promising candidates for TEGs because they have Seebeck coefficients larger than $100 \mu\text{V } ^\circ\text{C}^{-1}$.^[3d] Recently, a lightweight and flexible TEG module was demonstrated based on n-type bismuth telluride (Bi_2Te_3) and p-type antimony telluride (Sb_2Te_3).^[136] Thermoelectric thick film was firstly fabricated by screen-printing onto polyimide film, followed by PEDOT:PSS infiltration to form a hybrid composite. Incorporation of PEDOT:PSS into the screen-printed TE film significantly improved the flexibility of the film up to a bending radius of 3 cm without degradation of TE properties (Figure 17a,b). The flexible TEG module fabricated by this technique has produced high output power density of 1.2 mW cm^{-2} at a 50 K temperature difference. To demonstrate the mechanical endurance and potential for wearable energy applications, a TEG consisting of seven thermoelectric couples was subjected to cyclic mechanical bending (radius of curvature of 4 cm) of over 1000 cycles. The fatigue strength of the device was shown in Figure 17c, with only minimal increase in resistance. The mechanical compliance of the TEGs could be further improved by screen printing dots of Bi_2Te_3 and Sb_2Te_3 onto a woven glass fabric and subsequently sealed inside a PDMS encapsulate (Figure 17d).^[137] The mechanically compliant glass fabric substrate not only served as support for the thermoelectric materials that sustained the printed patterns, but also increased power generation by interrupting phonon propagation.^[137] A high-performance TEG exhibited a high output power density of 3.8 mW cm^{-2} and 28 mW g^{-1} at a $\Delta T = 50\text{K}$. For further demonstration of the use of the flexible TE generator on the human body, a bandage-like flexible glass fabric TE generator with 11 TE couples was designed and applied to human skin as a body heat energy harvester. The TE module generates an open-circuit output voltage of 2.9 mV and an output power of 3 μW on a matched external load at an air temperature of 15 $^\circ\text{C}$. The device showed no significant change ($<5\%$) in the internal resistance with the allowed bending radius of 20 mm (Figure 18e). Meanwhile, the resistance of the device is almost unchanged when repeatedly bent up to 120 cycles with a radius of curvature of 50 mm was applied (Figure 18f).

5. Energy Devices for Wearable and Implantable Biomedical Applications

5.1. Human/Device Interface Design

It is encouraging to see significant advances in the development of stretchable ESCDs using various materials and strategies, which lay solid theoretical frameworks toward future wearable and implantable energy devices. Additional requirements for realizing such energy devices in the real world include the consideration of compatibility of existing stretchable ESCDs with biological materials, long-term durability in biological conditions, and potential immune response.^[138] In this context, the interface between the ESCDs and human skin/tissue becomes significant. While much attention has been paid to the flexibility and stretchability of ESCDs with various design layouts, the materials interface with human skin/tissue has not yet drawn much attention until recently. The majority

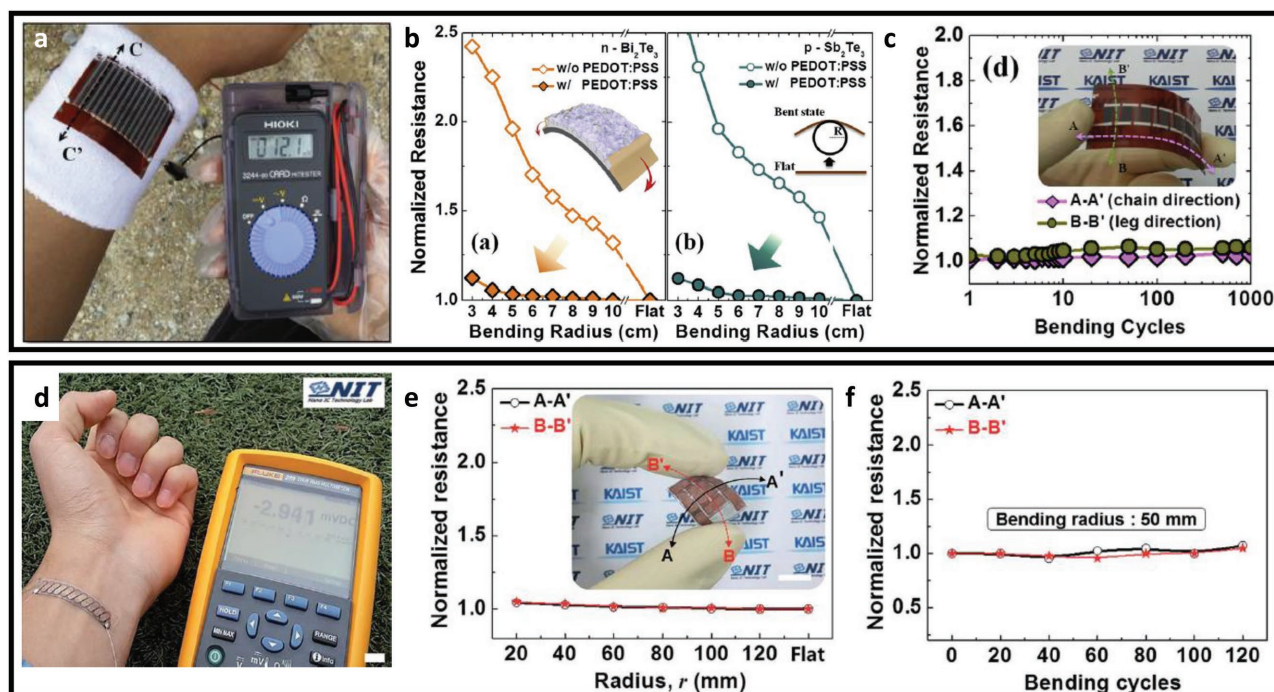


Figure 17. a) Photograph of a wearable hybrid inorganic–organic composite thermoelectric generator onto wrist support. b) Normalized resistance changes before (open points) and after (closed points) PEDOT:PSS infiltration as a function of bending radius for Bi_2Te_3 (left) and Sb_2Te_3 (right). c) Resistance changes of the module as a function of the number of bending cycles with a bending radius of 40 mm. Reproduced with permission.^[136] Copyright 2014, Elsevier Ltd. d) Electricity generation measured on human skin at an air temperature of 15 °C. Scale bar, 1 cm. e) Resistance stability of the device under bending stress along two bending axes as a function of bending radius. f) Stability of 120 bending cycles at bending radius of 50 mm. Reproduced with permission.^[137] Copyright 2014, Royal Society of Chemistry.

of current energy devices, in spite of their high stretchability, are typically too bulky to be body-worn as real-world wearable energy devices. Several strategies have recently been proposed for the human/device interfaces, including superthin epidermal design,^[139] skin-conformal microhairy design,^[140] and mechanical adaptive design.^[138]

The mechanics and soft adhesion chemistry at the biotic/abiotic interface are the key considerations for the integration of soft energy devices with human skins. An analytical mechanics model in which the skin surface morphology is assumed to be sinusoidal with a characteristic amplitude and wavelength.^[4d] The critical materials/device thickness below which van der Waals forces are sufficiently strong to drive perfect, conformal contact can be determined by considering the total energy associated with interfacial contact ($U_{\text{interface}}$) as:^[141]

$$U_{\text{interface}} = U_{\text{substrate_bending}} + U_{\text{skin_elasticity}} + U_{\text{adhesion}} \quad (8)$$

where $U_{\text{substrate_bending}}$, $U_{\text{skin_elasticity}}$, and U_{adhesion} are the bending energy of the substrate, the elastic energy of the skin, and the adhesion energy, respectively. Conformal contact results when the adhesion energy is larger than the sum of the bending and the elastic energies.^[4d,140] Based on this model, a firm interface between biotic and abiotic system could be achieved in the effort of reducing materials/device thickness and increasing adhesion energy. As shown in Figure 18a, a 5- μm -thick epidermal electronic membrane makes excellent conformal contact with a polymer surface moulded into the shape of human skin

(forearm).^[142] At a thicknesses of 36 μm , 100 μm , and 500 μm , air gaps can be observed at the interface with decreasing contact areas when a thicker film is applied.^[4d] Examples include an epidermal supercapacitor with overall device thickness of only 1 μm based on a SWCNT/PEDOT hybrid film (100–200 nm in thickness).^[139] The as-designed supercapacitors could be interfaced with human skin with conformal bonding and outstanding flexibility.

Efforts have also been devoted to enhance the adhesion energy of substrates by devising hairy microstructures.^[140,143] In this configuration, the aspect ratio of the microhair structure needs to be higher than a critical value to form a stable contact with the skin.^[143] As indicated in Figure 18b, substrates with flat geometry and microhair structures with a low aspect ratio of 3 and 6 showed both macro- and micro-sized voids to pig skin, whereas the sensor with an aspect ratio of 10 microhair structures was contacted against the pig skin with excellent conformity, which provides enhanced adhesion force to enable conformal contact between skin and devices.^[140] In addition, substrates with advanced features, such as shape memory,^[139] self-healing,^[144] and biodegradability^[145] have also been designed and fabricated for implantable ESCDs applications.

5.2. Wearable Biomedical Applications

Energy devices integrated with clothes, glasses, watches, shoes, and skin will bring new opportunities to sustainably drive

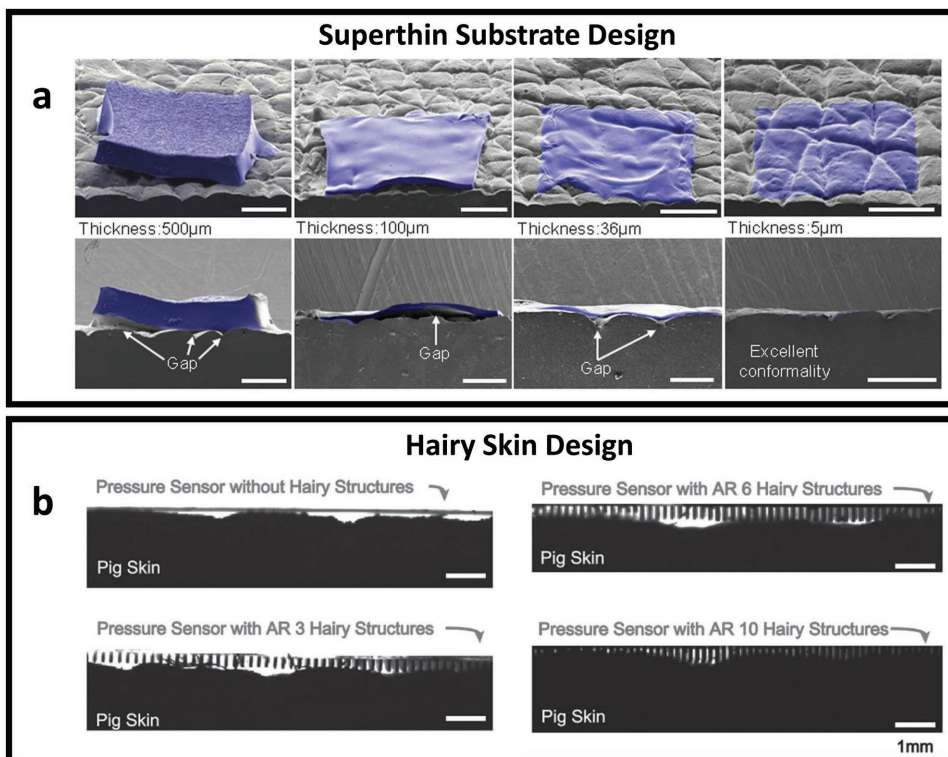


Figure 18. a) Angled and cross-sectional SEM images showing degree of conformal contact between a silicone replica of the surface of the skin (grey) and various thicknesses of elastomer membrane substrates (blue). Scale bar: 1 mm. Reproduced with permission.^[144] Copyright 2013, Wiley-VCH. b) Cross-sectional profiles of substrates with flat geometry and PDMS microhair structures with AR of 3, 6, and 10 attached on a pig skin with an applied load of 1 kPa. Reproduced with permission.^[143] Copyright 2015, Wiley-VCH.

wearable biomedical electronics. Although recent research establishes an impressive variety of options in energy storage (batteries and supercapacitors) and generation (piezoelectric, triboelectric, thermoelectric, and photovoltaic devices),^[146] the practical use of such devices is still limited because of poor durability of active materials under repeated mechanical deformation, human-skin/device interface delamination, or short life span of the energy devices. To address the current challenges, several power systems are proposed with the aim of simultaneously collecting, storing, and using electricity for biomedical devices anytime, anywhere.

Rechargeable and wearable textile energy devices could be easily integrated with cloth and wrist watches^[147,148] (Figure 19a,b) thus showing great promise for the power supply of wearable biomedical applications. Such a system was realized by integrating Ni-coated polyester yarn as a current collector, polyurethane (PU) binder for strong adhesion of active materials, and PU separator with superior mechanical and electrochemical properties.^[147] The sheet resistance of the Ni-coated textile reaches $0.35 \Omega \text{ sq}^{-1}$, which is significantly lower than their carbon-based counterparts. The textile battery retained 91.8% of the original capacity after 40 cycles folding-unfolding cycles with bending radius down to 0.65 mm, indicating that the overall electrochemical reaction remains preserved under large mechanical deformations. In addition, a series of flexible and lightweight polymer solar cells are integrated on the pouch of the wearable textile battery for more convenient charge of the

wearable textile battery. The integration of flexible solar cells with the wearable battery would relieve the capacity requirement substantially for biomedical devices, as the operation hours of the electronics are not restricted by the total capacity during the solar cell operation in daytime.^[147]

Another power management system uses thin, soft, and skin-compatible means for direct integration with the human body.^[146] The system combined dual-junction compound semiconductor, millimeter-scale solar cells with bare die, chip-scale rechargeable lithium-ion batteries, integrated circuits for power management, and advanced near-field communication (NFC) module for wireless data processing. Optimized geometries in the serpentine wiring afford system-level, elastic biaxial stretchability up to 30% with a low effective modulus. In addition, the design offered considerable versatility in electrical output characteristics. As an example, a solar module that involves a 4×4 array of 2J solar cells all connected in series produces open-circuit voltages and shortcircuit currents of 33.1 V and -1.59 mA , respectively, with a maximum power of 43.0 mW. Similarly, a 4×4 array of chip-scale batteries connected in parallel exhibit a discharge current of $500 \mu\text{A}$ and maximum power of 77.3 mW for 20 mA output for $\approx 2 \text{ min}$.^[146] These power levels can satisfy practical requirements in several recently demonstrated types of stretchable skin-mounted biomedical devices. The power management system was further exploited in a skin-mounted, wireless sensor system for autonomous skin thermography. The systems were mounted onto the forearm of a subject during

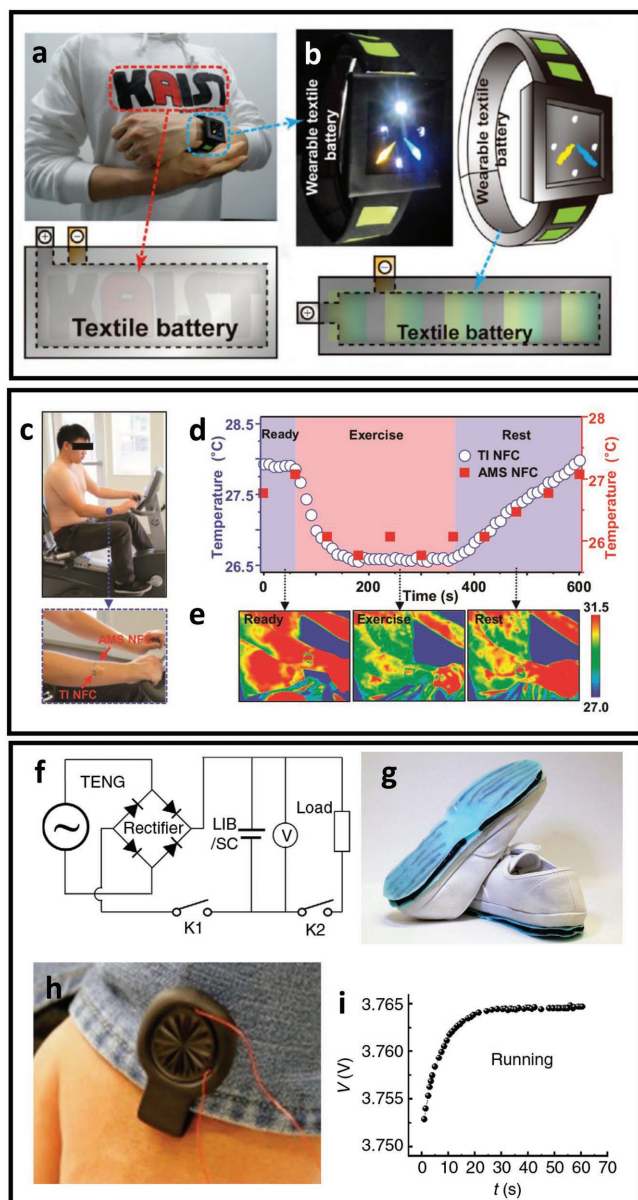


Figure 19. a) A photograph of wearable textile battery embedded in clothes together with its enlarged view of the inner cell structure. b) Photograph and schematic representation of a watch with a wearable textile battery strap. Reproduced with permission.^[147] Copyright 2013, American Chemical Society. c) Optical images of a device laminated onto the forearm of a subject during exercise on a stationary bike. d) Temperature data recorded immediately before (“ready”), during (“exercise”), and immediately after (“rest”) exercise on the bike. e) Infrared radiation images corresponding to each stage of the evaluation. Reproduced with permission.^[146] Copyright 2016, National Academy of Sciences. f) Circuit diagram of a self-charging power system integrated by the TENG and supercapacitor/lithium-ion battery. g) Image of the self-charging ‘energy-shoe’. h–i) A fitness tracker (h) is driven and LIB is charged (i) simultaneously by the ‘energy-shoe’ when jogging. Reproduced with permission.^[149] Copyright 2016, Nature Publishing Group.

exercise on a stationary bike (Figure 19c) at a sampling rate of 1 point/10 s over 10 min. A separate wirelessly powered NFC device placed on an adjacent region of the arm collected data

at a sampling rate of 1 point/1 min to provide a set of data as a control. The data (Figure 19d) show variations in temperature during “ready,” “exercise,” and “rest” stages, with high consistency between battery powered devices and wirelessly powered devices. Figure 19e showed the infrared camera images under the three conditions for an additional point of comparison.

To further extend the life span of energy devices and ensure a continuous power supply beyond daytime, integrated nano-generators that harvest biomechanical energy have been used for state-of-the-art wearable energy-management systems.^[149] The wearable power source is realized via a TENG with a rationally designed helix–belt contact structure, which is then packaged with a layer of silicone rubber for waterproofing and anticorrosive purposes. The surface charge density of the helix–belt structure is about 250 mC, and the output charges can be linearly adjusted according to the load of the electronics by using multiple TENG tubes in parallel. The TENG tubes can be further integrated with a supercapacitor/LIB to form a self-charging power system (Figure 19f). Moreover, the geometry of the TENG can be tailored to meet customers’ requests. For example, 40 tubes were assembled under a pair of shoes (Figure 19g), with the capability to sustainably powered a wearable fitness tracker (Figure 19h) sorely by walking and jogging. The original batteries of the electronic devices are replaced in advance by a homemade LIB, with the LiMn_2O_4 active material of 0.5 mg that is specially designed for the TENG to ensure a fast charging rate. The self-charging power system is also able to support the electronic device and charge the LIB simultaneously (Figure 19i).^[149]

Another energy management system uses textile based energy devices to collect outdoor sunshine and random body motion energies simultaneously in an energy storage unit.^[150] Both types of energies can be easily converted into electricity by using fiber-shaped dye-sensitized solar cells (for solar energy) and fiber-shaped triboelectric nanogenerators (for random body motion energy), and then further stored as chemical energy in fiber-shaped supercapacitors. An open-circuit voltage of 0.74 V and a short-circuit current density of 11.92 mA cm^{-2} were achieved for a single fiber-shaped dye-sensitized solar cell unit, corresponding to an overall power conversion efficiency of 5.64%. The F-TENG could deliver an output current of up to 0.91 mA. The supercapacitor unit exhibits a promising specific capacitance (1.9 mF cm^{-1}), which makes it an effective energy system to operate wearable biomedical devices.

5.3. Implantable Biomedical Applications

Implantable medical devices require electrical power to function within the body, which is more difficult to achieve because of additional requirements like tissue-attachability, long lifetime, biocompatibility, wireless power charging, and biodegradability.^[4b,151,152] Impressive progress has been achieved in recent years by using biofuel cells^[153,154] and silicon solar cells^[155,156] to power in vivo biomedical devices including pacemakers and stimulators with a relatively stiff or rigid layout. However, implantable energy systems in more flexible forms are highly sought after to avoid adverse side effects of the body.^[152] In addition, energy systems are desired to harvest power

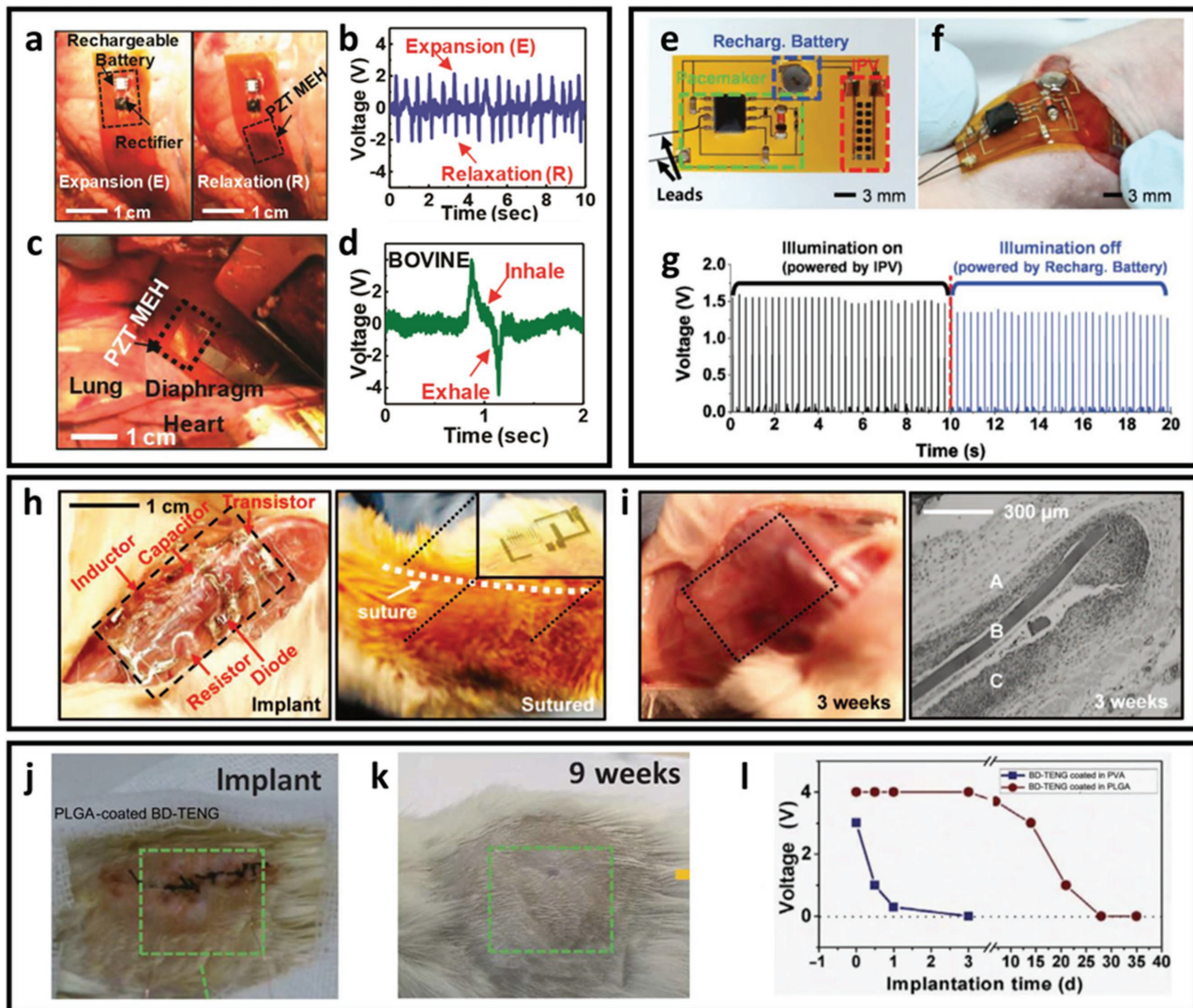


Figure 20. a) Photographs of a PZT mechanical energy harvester co-integrated with a rectifier and rechargeable battery, mounted on the right ventricle of a bovine heart during expansion (Left) and relaxation (Right). b) Open-circuit voltage as a function of time for PZT mechanical-energy harvesters mounted on right ventricle. c) Photograph of a PZT mechanical-energy harvester on the bovine diaphragm. d) Voltage as a function of time for the device on the bovine diaphragm. Reproduced with permission.^[4b] Copyright 2014, National Academy of Sciences. e) Photograph of a flexible cardiac pacemaker integrated with the implanted photovoltaic device and a rechargeable battery. f) A photograph during surgical procedure to implant the IPV device under the back skin of a mouse. g) Output impulses (≈ 3 Hz) from the subdermally implanted self-powered pacemaker powered by the IPV device under the skin. e–g) Reproduced with permission.^[151] Copyright 2016, Wiley-VCH. h) Images of an implanted (left) and sutured (right) demonstration platform for transient electronics located in the subdermal dorsal region of a BALB/c mouse. i) Implant site (left) and histological section (right) of tissue at the implant site after 3 weeks. Reproduced with permission.^[157] Copyright 2012, American Association for the Advancement of Science. j–k) Photographs of an implanted demonstration for BD-TENG located in the subdermal dorsal region of a rat. j) Implant site right after suture. k) Implant site after 9 weeks. l) Plotted electrical output of BD-TENGs at several time intervals after implantation. Reproduced with permission.^[152] Copyright 2016, American Association for the Advancement of Science.

throughout the macroscale displacement cycles associated with natural motions of an organ,^[4b] as charging or replacing a battery may require additional surgeries to the wearer.

In 2014, a flexible PZT-based thin-film generator was designed to harvest bio-mechanical energy from cardiac and lung motions.^[4b] The key functional element is a capacitor-type structure that consists of a layer of PZT (500 nm) between bottom (Ti/Pt, 20 nm/300 nm) and top (Cr/Au, 10 nm/200 nm) electrodes. The generator consists of 12 groups of PZT structures in series to increase the output voltage. The harvested

energy could be captured directly by use of a chip-scale rechargeable battery and a Schottky bridge rectifier integrated on the same flexible substrates with PZT mechanical energy harvester (MEH). In vivo testing was undertaken by attaching and anchoring the flexible energy system onto different areas of bovine's heart and lung to harvest bio-mechanical energy (Figure 20a,c).^[4b] Analysis of voltage outputs during periodic motion of heart and lung was illustrated in Figure 20b,d, respectively. These results indicate that flexible PZT mechanical-energy-harvester systems are readily capable of harnessing

energy from different locations across the body. Furthermore, the time-averaged power density of the unit corresponds to $0.18 \mu\text{W cm}^{-2}$ for mounting on the right ventricle 45° of bovine's heart, which is enough to power state-of-the-art pacemakers with average power consumption values as low as $0.3 \mu\text{W}$.^[4b]

Another implantable energy harvesting system based on flexible subdermal solar cell arrays was recently demonstrated.^[151] This approach takes the advantage of the transparency or translucency of skin or tissues to power implantable devices by converting solar energy to electricity. The thin film flexible solar cell arrays were fabricated by sputtering metal interconnects to the array of ultrathin dual-junction solar microcells (GaInP/GaAs with thickness of $5.7 \mu\text{m}$) that is transfer-printed on the flexible polyimide film. The devices are finally encapsulated with multiple layers of biocompatible and transparent polymers, which provide a thin and flexible structure to be more mechanically compatible with skin. Such subdermal solar cell arrays exhibited a typical short-circuit current density of 2.6 mA cm^{-2} , maximum power density of 10 mW cm^{-2} , and conversion efficiency of 10% after being implanted into live mouse models, which can power various types of assistive electronics within body. Figure 20e,f shows an example of a subdermally implantable flexible pacemaker integrated with the inorganic photovoltaic device (IPV) and rechargeable battery. The IPV device under the skin can supply about $\approx 195 \mu\text{A}$ of current to the pacemaker when light source is available, resulting in a continuous electrical impulses (Figure 20g, left). The implanted pacemaker can also be powered with a battery that is recharged by the IPV device when the light source is not available (Figure 20g, right).^[151]

Biodegradable energy management systems have also drawn intensive attention in recent years for implantable applications. The devices can be degraded and resorbed in the body, so no operation is needed to remove them, and adverse long-term side effects are avoided. Silicone-based devices are highly desirable for such applications as most of the traditional implantable biomedical components including sensors, actuators, power supplies, and wireless control systems are based on silicone-wafer substrates. In 2012, a system combined with single crystalline nanomembranes of silicon (Si NMs) and other dissolvable metals (e.g., Zn, Fe, W, Mo) was introduced,^[157] to achieve not only the essential electronic components needed for integrated circuits but also energy devices such as solar cells,^[157] energy harvesters,^[158] and primary batteries.^[145] Specifically, Ultrathin Si solar cells ($\approx 3 \text{ mm}$ thick) with fill factors of 66% and overall power conversion efficiencies of $\approx 3\%$ was achieved even without light-trapping structures, backside reflectors, or antireflection coatings.^[157] Bendable piezoelectric energy harvesters based on dissolvable ZnO could provide output power density of $\approx 10 \text{ nW cm}^{-2}$ during cycles of bending.^[158] In addition, the biodegradable Mg battery exhibits stable voltage (0.4–0.7 V), higher discharge current density (0.1 mA cm^{-2}), and higher specific capacity (276 mA h g^{-1}) simultaneously, which could drive a wireless implantable sensing platform ($< 5 \mu\text{W}$) for 1 month with a battery thickness of only $30 \mu\text{m}$.^[145] Ultraflexible or stretchable configurations of transient electronics were also achieved by using biodegradable elastomers and Mg electrodes with serpentine design, where the device structures won't delaminate before stretching to more than

30%.^[159] To demonstrate the biodegradability, transient devices were implanted in the subdermal region of BALB/c mice (Figure 20h).^[157] The integrated after 3 weeks (Figure 20i, left) revealed only faint residues, with evidence of slow reintegration into the subdermal layers, along with apparent revascularization. The histological section in Figure 20i (right) shows the subdermal layer (A), the silk film (B), and the muscle layer (C) and reveals no significant inflammatory reactions.^[157]

Another example is an biodegradable TENG (BD-TENG) for short-term, in vivo biomechanical-energy conversion.^[152] Four biodegradable polymers were selected: poly(L-lactide-co-glycolide) (PLGA), poly(3-hydroxybutyric, acid-co-3-hydroxyvaleric acid) (PHB/V), poly(caprolactone) (PCL), and poly(vinyl alcohol) (PVA). The as-fabricated device consists of two selected biodegradable polymer (BDP) layers (PLGA, PVA, PCL, and PHB/V) with patterned nanoscale surface structures were assembled together as friction parts with a spacer ($200 \mu\text{m}$) in between. A thin Mg film (50 nm) was deposited on one side of each friction layer as an electrode layer. The whole structure was finally encapsulated in BDP with thickness of $100 \mu\text{m}$. The device reached optimized open-circuit voltage (V_{oc}) ($\approx 40 \text{ V}$) and short-circuit current (I_{sc}) ($\approx 1 \text{ mA}$) when PLGA and PCL were chosen as friction parts. To demonstrate the potential for in vivo applications, two representative BD-TENGs were implanted in the subdermal region of rats (Figure 20h). The wound healed well with no obvious infection after 9 weeks of implantation (Figure 20i), revealing good biocompatibility of BD-TENGs. The output performance of BD-TENGs was decreased from 4 to 1 V after 2 weeks of implantation, possibly due to the restriction of a fibrous capsule surrounding the BD-TENG and the swelling of the encapsulation layer. The electrode wires fell off at week 4 after encapsulation layer being infiltrated by water. The integrity of the structure was destroyed after 9 weeks of implantation, indicating that most materials were biodegraded in the animal body. In comparison, PVA-coated BD-TENGs could work for over 24 hours in vivo (output, $\approx 3 \text{ V}$) and almost dissolved completely within 72 hours (Figure 20j).^[152]

6. Summary

Current wearable and/or implantable electronic devices are 'energy-hungry', which calls for urgent solutions for seamlessly integrating energy devices with biological systems to power such kinds of devices, ideally for the lifetime of the living organisms. In contrast to dominant research efforts in worldwide, big energy sectors with the goal of improving energy density and/or power density, little attention has been paid to wearable or implantable energy research, until recently. In the context of wearable or implantable energy systems, the challenges are soft/hard materials interfaces between typically rigid active materials and soft biological skins/tissues, durability in biological environments, integrateability with other components such as sensors and wireless circuits, etc. Unlike conventional materials-focused energy research, wearable/implantable energy research often requires multidisciplinary collaborations among scientists, engineers, IT, and clinicians. A summary of wearable and implantable energy-management system is presented in **Table 1**.

Table 1. Summary of wearable and implantable energy management systems.

Applications	Configurations	Flexibility	Electrical power input	Electrical power output	Reference
Wearable biomedical applications	LIBs; solar cells	30% biaxial strain	12.5 mW	2.4–4.5 V; 100 μ A	[146]
	Textile LIBs; solar cells	$R_c^{a)}$ = 0.65 mm	10 mA cm ⁻²	0.6–2.4 V; 85 mA g ⁻¹	[147]
	Stretchable TENGs; LIBs	100% uniaxial strain	21 μ A	700 μ A	[148]
	TENGs; LIBs; supercapacitors	150% uniaxial strain	250 μ C m ⁻²	2.8–4.2 V	[149]
	TENGs; solar cells; supercapacitors	Bendable	11.92 mA cm ⁻²	1.8 V	[150]
Implantable biomedical applications	PZT MEH; rechargeable battery	Bendable	0.18 μ W cm ⁻²	4.5 V	[4b]
	IPV; rechargeable battery	Bendable	10 mW cm ⁻²	6.5 μ Ah; 2–3.3 V	[151]
	Si solar cell	Bendable	10 mA cm ⁻²	N/A	[157]
	Piezoelectric energy harvesters	Bendable	10 nW cm ⁻²	N/A	[158]
	Mg primary batteries	Fordable	N/A	0.1 mA cm ⁻²	[145]
	BD-TENGs	Bendable	32.6 mW m ²	N/A	[152]

^{a)} R_c : bending radius.

This article systematically reviews recent progress that has been made in the development of stretchable energy storage and conversion devices toward powering future wearable and implantable biomedical electronics. Choices of active materials including carbon nanotubes, graphene, conductive polymers, metal nanoparticles/nanowires, and hybrid materials have been discussed in details. Their interactions with elastomeric substrates and supporting electrolytes have also been described. Novel materials properties such as intrinsic stretchability, self-healing, biodegradability, skin-adhesiveness, and optical transparency have been utilized in novel energy storage and conversion devices.

Stretchability is one of key requirement, in which we have covered two dominant strategies, namely structures that stretch (STS) and materials that stretch (MTS). The former may include buckling design, serpentine design, origami design, and textile/porous design; the latter may involve in the usage of nanomaterials incorporated into or onto elastomeric substrates. In either case, soft/hard materials interfaces are the key considerations for preventing materials from delamination/cracking, which are the key governing parameters affecting the efficiency of wearable energy generation or conversion. We have also briefly discussed biocompatibility issues, which have not yet addressed much currently, but will be essential for future biointegrated medical devices.

In addition to the above energy devices, wireless charging is gaining popularity in implantable systems. A flexible platform that incorporates advanced optoelectronic functionality for applications in wireless capture and transmission of photoplethysmograms without the use of a battery has been demonstrated.^[160] Such a novel energy supplying technique in conjunction with advanced features, such as self-healing, biodegradable, super-thinness, and mechanical adaptability may represent important directions for future implantable systems.

7. Challenges and Opportunities

In spite of encouraging progress made to date, development of disruptive soft, elastic, wearable/implantable energy devices

with novel materials is still in the infancy stage. Ideally, a wearable/implantable energy device should be thin, elastic, and integratable with skins, muscles, and organs to be truly a part of the human body and to realize a self-sustainable system. The majority of current stretchable energy devices remain too bulky to be ‘unfeetable’ and ‘unseeable’ wearables.

As for stretchable energy storage devices including supercapacitors and batteries, it remains important to discover novel active materials with enhanced electrochemical and mechanical performances and improved safety. Scale up synthesis of these materials at the industry scale is also important for future real-world applications. It is also important to develop durable and biocompatible electrolytes with high ionic conductivities for their uses in energy storage applications. In addition, development of the packaging materials with integration of active materials, electrolytes, and elastomeric substrates is imperative, but has not yet attracted much attention.

Wearable photovoltaic devices represent a renewable solution, but their power output is subject to the availability and the intensity of light sources. They may hardly provide a continuous, stable, and long-lasting power supply to wearable and implantable electronics. A possible solution is to develop an integrated energy system with a combination of stretchable photovoltaic devices and stretchable energy storage devices, thus excess energy can be stored in the day time. In addition, few examples of photovoltaic devices that can withstand significant strains without intentional, out-of-plane buckling design due to multilayers of different types of materials are typically needed in photovoltaic system.

Conversion of biomechanical energy into electricity is appealing for wearable or implantable electronics because energy can be, in principle, generated on demand. This can be achieved either by the piezoelectric or triboelectric effect. Compared with flexible piezoelectric devices, triboelectric energy harvesters have much higher power densities with the highest reported value of ≈ 50 mW cm⁻². Therefore, triboelectric energy devices are advantageous for integration with batteries or supercapacitors to create practical power sources for wearable and implantable electronics. Although the power output performance of triboelectric devices has been significantly

improved through introduction of new materials and surface engineering technologies, challenges still exist prior to real-world applications. For instance, the required gap and the air exchange during mechanical deformation make the package of stretchable triboelectric generators rather challenging, particularly for implantable systems, albeit spacers can be avoided in some cases.^[161]

As far as wearable thermoelectric generators are concerned, their power factors are so low such that the temperature difference between human body and air generates only millivolt level voltage and a power density of only a few $\mu\text{W cm}^{-2}$. Therefore, a large number of thermoelectric generators are required to be connected in serial to achieve the required voltage to power wearable biomedical devices, which will inevitably increase volume and weight of devices—a situation not favourable for wearable electronics. Fundamental understanding of how mechanical deformation affects long-term energy generation under biological conditions is rather limited.

In addition, other remaining challenges may include scalable low-cost manufacturing, packaging of energy devices, durability under long-term biological conditions, and seamless integration between energy devices and other components including sensors and wireless circuits. In order to address these challenges, novel materials innovation is the key to breakthrough technologies. Nevertheless, multidisciplinary collaboration is crucial, particularly collaboration among materials science, electronics, and biology is a must.

Acknowledgements

This work is financially supported by ARC discovery projects DP140100052 and DP150103750. This work was performed in part at the Melbourne Centre for Nanofabrication (MCN) in the Victorian Node of the Australian National Fabrication Facility (ANFF).

Conflict of Interest

The authors declare no conflict of interest.

Keywords

biomedical, energy conversion, energy storage, stretchable, wearable electronics

Received: March 9, 2017

Revised: April 11, 2017

Published online: July 17, 2017

- [1] a) J. A. Rogers, T. Someya, Y. Huang, *Science* **2010**, 327, 1603; b) M. L. Hammock, A. Chortos, B. C. K. Tee, J. B. H. Tok, Z. Bao, *Adv. Mater.* **2013**, 25, 5997; c) Z. Fan, J. C. Ho, T. Takahashi, R. Yerushalmi, K. Takei, A. C. Ford, Y. L. Chueh, A. Javey, *Adv. Mater.* **2009**, 21, 3730; d) F. R. Fan, W. Tang, Z. L. Wang, *Adv. Mater.* **2016**, 28, 4283; e) S. Wagner, S. Bauer, *MRS Bull.* **2012**, 37, 207; f) A. Chortos, J. Liu, Z. Bao, *Nat. Mater.* **2016**, 15, 937; g) T. Someya, Z. Bao, G. G. Malliaras, *Nature* **2016**, 540, 379.

- [2] T. F. O'Connor, S. Savagatrup, D. J. Lipomi, in *Stretchable Bioelectronics for Medical Devices and Systems*, (Eds: J. A. Rogers, R. Ghaffari, D.-H. Kim), Springer, **2016**.
- [3] a) C. Yan, P. S. Lee, *Small* **2014**, 10, 3443; b) K. Xie, B. Wei, *Adv. Mater.* **2014**, 26, 3592; c) S. Pan, J. Ren, X. Fang, H. Peng, *Adv. Energy Mater.* **2015**, 6, 1501867; d) H. Wu, Y. Huang, F. Xu, Y. Duan, Z. Yin, *Adv. Mater.* **2016**, 28, 9881; e) L. Dong, C. Xu, Y. Li, Z.-H. Huang, F. Kang, Q.-H. Yang, X. Zhao, *J. Mater. Chem. A* **2016**, 4, 4659; f) D. J. Lipomi, Z. Bao, *Energy Environ. Sci.* **2011**, 4, 3314; g) Y. Zhang, Y. Huang, J. A. Rogers, *Curr. Opin. Solid State Mater. Sci.* **2015**, 19, 190; h) Y. Shao, M. F. El-Kady, L. J. Wang, Q. Zhang, Y. Li, H. Wang, M. F. Mousavi, R. B. Kaner, *Chem. Soc. Rev.* **2015**, 44, 3639; i) T. Lv, Y. Yao, N. Li, T. Chen, *Nano Today* **2016**, 11, 644.
- [4] a) P. P. Mercier, A. C. Lysaght, S. Bandyopadhyay, A. P. Chandrakasan, K. M. Stankovic, *Nat. Biotechnol.* **2012**, 30, 1240; b) C. Dagdeviren, B. D. Yang, Y. Su, P. L. Tran, P. Joe, E. Anderson, J. Xia, V. Doraiswamy, B. Dehdashti, X. Feng, B. Lu, R. Poston, Z. Khalpey, R. Ghaffari, Y. Huang, M. J. Slepian, J. A. Rogers, *Proc. Natl. Acad. Sci. U.S.A.* **2014**, 111, 1927; c) A. J. Bandodkar, W. Jia, C. Yardimci, X. Wang, J. Ramirez, J. Wang, *Anal. Chem.* **2014**, 87, 394; d) J. W. Jeong, W. H. Yeo, A. Akhtar, J. J. Norton, Y. J. Kwack, S. Li, S. Y. Jung, Y. Su, W. Lee, J. Xia, H. Cheng, Y. Huang, W. Choi, T. Bretl, J. A. Rogers, *Adv. Mater.* **2013**, 25, 6839; e) S. Gong, W. Schwalb, Y. Wang, Y. Chen, Y. Tang, J. Si, B. Shirinzadeh, W. Cheng, *Nat. Commun.* **2014**, 5, 3132; f) M. A. Rosa, S. H. Lisanby, *Neuropsychopharmacology Rev.* **2012**, 37, 102; g) T. Yokota, P. Zalar, M. Kaltenbrunner, H. Jinno, N. Matsuhisa, H. Kitano, Y. Tachibana, W. Yukita, M. Koizumi, T. Someya, *Sci. Adv.* **2016**, 2, e1501856; h) H. C. Ko, M. P. Stoykovich, J. Song, V. Malyarchuk, W. M. Choi, C.-J. Yu, J. B. Geddes, J. Xiao, S. Wang, Y. Huang, J. A. Rogers, *Nature* **2008**, 454, 748.
- [5] D.-H. Kim, J. Song, W. M. Choi, H.-S. Kim, R.-H. Kim, Z. Liu, Y. Y. Huang, K.-C. Hwang, Y.-w. Zhang, J. A. Rogers, *Proc. Natl. Acad. Sci. U.S.A.* **2008**, 105, 18675.
- [6] D.-Y. Khang, H. Jiang, Y. Huang, J. A. Rogers, *Science* **2006**, 311, 208.
- [7] N. Bowden, S. Brittain, A. G. Evans, J. W. Hutchinson, G. M. Whitesides, *Nature* **1998**, 393, 146.
- [8] S. Yao, Y. Zhu, *Adv. Mater.* **2015**, 27, 1480.
- [9] H. Jiang, D.-Y. Khang, J. Song, Y. Sun, Y. Huang, J. A. Rogers, *Proc. Natl. Acad. Sci. U.S.A.* **2007**, 104, 15607.
- [10] J. Jones, S. P. Lacour, S. Wagner, Z. Suo, *J. Vac. Sci. Technol.* **2004**, 22, 1723.
- [11] Y. Sun, W. M. Choi, H. Jiang, Y. Y. Huang, J. A. Rogers, *Nat. Nanotechnol.* **2006**, 1, 201.
- [12] C. Yu, C. Masarapu, J. Rong, B. Wei, H. Jiang, *Adv. Mater.* **2009**, 21, 4793.
- [13] a) Z. Niu, H. Dong, B. Zhu, J. Li, H. H. Hng, W. Zhou, X. Chen, S. Xie, *Adv. Mater.* **2013**, 25, 1058; b) X. Chen, H. Lin, P. Chen, G. Guan, J. Deng, H. Peng, *Adv. Mater.* **2014**, 26, 4444.
- [14] T. Chen, Y. Xue, A. K. Roy, L. Dai, *ACS Nano* **2013**, 8, 1039.
- [15] C. Wang, W. Zheng, Z. Yue, C. O. Too, G. G. Wallace, *Adv. Mater.* **2011**, 23, 3580.
- [16] a) W. M. Choi, J. Song, D.-Y. Khang, H. Jiang, Y. Y. Huang, J. A. Rogers, *Nano Lett.* **2007**, 7, 1655; b) D.-H. Kim, J.-H. Ahn, W. M. Choi, H.-S. Kim, T.-H. Kim, J. Song, Y. Y. Huang, Z. Liu, C. Lu, J. A. Rogers, *Science* **2008**, 320, 507. c) J. Yu, W. Lu, S. Pei, K. Gong, L. Wang, L. Meng, Y. Huang, J. P. Smith, K. S. Booksh, Q. Li, J.-H. Byun, Y. Oh, Y. Yan, *ACS Nano* **2016**, 10, 5204.
- [17] J. Zang, S. Ryu, N. Pugno, Q. Wang, Q. Tu, M. J. Buehler, X. Zhao, *Nat. Mater.* **2013**, 12, 321.
- [18] J. Zang, C. Cao, Y. Feng, J. Liu, X. Zhao, *Sci. Rep.* **2014**, 4, 6492.
- [19] Z. Liu, S. Fang, F. Moura, J. Ding, N. Jiang, J. Di, M. Zhang, X. Lepró, D. Galvão, C. Haines, N. Y. Yuan, S. G. Yin, D. W. Lee, R. Wang,

- H. Y. Wang, W. Lv, C. Dong, R. C. Zhang, M. J. Chen, Q. Yin, Y. T. Chong, R. Zhang, X. Wang, M. D. Lima, R. Ovalle-Robles, D. Qian, H. Lu, R. H. Baughman, *Science* **2015**, 349, 400.
- [20] Y. Huang, M. Zhong, Y. Huang, M. Zhu, Z. Pei, Z. Wang, Q. Xue, X. Xie, C. Zhi, *Nat. Commun.* **2015**, 6, 10310.
- [21] a) D. Y. Khang, J. A. Rogers, H. H. Lee, *Adv. Funct. Mater.* **2009**, 19, 1526; b) J. Song, H. Jiang, Y. Huang, J. A. Rogers, *J. Vac. Sci. Technol. A* **2009**, 27, 1107.
- [22] a) H. Cheng, Y. Zhang, K.-C. Hwang, J. A. Rogers, Y. Huang, *Int. J. Solids Struct.* **2014**, 51, 3113; b) H. Jiang, D.-Y. Khang, H. Fei, H. Kim, Y. Huang, J. Xiao, J. A. Rogers, *J. Mech. Phys. Solids* **2008**, 56, 2585.
- [23] M. Gonzalez, F. Axisa, M. V. Bulcke, D. Brosteaux, B. Vandeveld, J. Vanfleteren, *Microelectron. Reliab.* **2008**, 48, 825.
- [24] Y. Zhang, S. Xu, H. Fu, J. Lee, J. Su, K.-C. Hwang, J. A. Rogers, Y. Huang, *Soft Matter* **2013**, 9, 8062.
- [25] Y. Zhang, S. Wang, X. Li, J. A. Fan, S. Xu, Y. M. Song, K. J. Choi, W. H. Yeo, W. Lee, S. N. Nazaar, B. Liu, L. Yin, K. Hwang, J. A. Rogers, Y. Huang, *Adv. Funct. Mater.* **2014**, 24, 2028.
- [26] J. Song, Y. Huang, J. Xiao, S. Wang, K. Hwang, H. Ko, D.-H. Kim, M. Stoykovich, J. Rogers, *J. Appl. Phys.* **2009**, 105, 123516.
- [27] S. Xu, Y. Zhang, J. Cho, J. Lee, X. Huang, L. Jia, J. A. Fan, Y. Su, J. Su, H. Zhang, H. Cheng, B. Liu, C. Yu, C. Chuang, T. Kim, T. Song, K. Shigeta, S. Kang, C. Dagdeviren, I. Petrov, P. V. Braun, Y. Huang, U. Paik, J. A. Rogers, *Nat. Commun.* **2013**, 4, 1543.
- [28] Y. Zhang, H. Fu, Y. Su, S. Xu, H. Cheng, J. A. Fan, K.-C. Hwang, J. A. Rogers, Y. Huang, *Acta Mater.* **2013**, 61, 7816.
- [29] J. A. Fan, W.-H. Yeo, Y. Su, Y. Hattori, W. Lee, S.-Y. Jung, Y. Zhang, Z. Liu, H. Cheng, L. Falgout, M. Bajema, T. Coleman, D. Gregoire, R. J. Larsen, Y. Huang, J. A. Rogers, *Nat. Commun.* **2014**, 5, 3266.
- [30] Z. Song, T. Ma, R. Tang, Q. Cheng, X. Wang, D. Krishnaraju, R. Panat, C. K. Chan, H. Yu, H. Jiang, *Nat. Commun.* **2014**, 5, 3140.
- [31] R. Tang, H. Huang, H. Tu, H. Liang, M. Liang, Z. Song, Y. Xu, H. Jiang, H. Yu, *Appl. Phys. Lett.* **2014**, 104, 083501.
- [32] Q. Cheng, Z. Song, T. Ma, B. B. Smith, R. Tang, H. Yu, H. Jiang, C. K. Chan, *Nano Lett.* **2013**, 13, 4969.
- [33] P.-K. Yang, Z.-H. Lin, K. C. Pradel, L. Lin, X. Li, X. Wen, J.-H. He, Z. L. Wang, *ACS Nano* **2015**, 9, 901.
- [34] a) C. Wu, X. Wang, L. Lin, H. Guo, Z. L. Wang, *ACS Nano* **2016**, 10, 4652; b) Z. Song, X. Wang, C. Lv, Y. An, M. Liang, T. Ma, D. He, Y.-J. Zheng, S.-Q. Huang, H. Yu, H. Jiang, *Sci. Rep.* **2015**, 5, 10988.
- [35] a) C. Lv, D. Krishnaraju, G. Konjevod, H. Yu, H. Jiang, *Sci. Rep.* **2014**, 4, 5979; b) Z. Y. Wei, Z. V. Guo, L. Dudte, H. Y. Liang, L. Mahadevan, *Phys. Rev. Lett.* **2013**, 110, 215501.
- [36] S. Zhai, H. E. Karahan, L. Wei, Q. Qian, A. T. Harris, A. I. Minett, S. Ramakrishna, A. K. Ng, Y. Chen, *Energy Storage Mater.* **2016**, 3, 123.
- [37] L. Hu, M. Pasta, F. L. Mantia, L. Cui, S. Jeong, H. D. Deshazer, J. W. Choi, S. M. Han, Y. Cui, *Nano Lett.* **2010**, 10, 708.
- [38] a) H. Lin, R. Ramgulam, H. Arshad, M. Clifford, P. Potluri, A. Long, *Comput. Mater. Sci.* **2012**, 65, 276; b) A. Hallal, R. Younes, F. Fardoun, *Composites Part B* **2013**, 50, 22.
- [39] X. Yu, X. Su, K. Yan, H. Hu, M. Peng, X. Cai, D. Zou, *Adv. Mater. Technol.* **2016**, 1, 1600009.
- [40] T. G. Yun, M. Oh, L. Hu, S. Hyun, S. M. Han, *J. Power Sources* **2013**, 244, 783.
- [41] C. Choi, J. M. Lee, S. H. Kim, S. J. Kim, J. Di, R. H. Baughman, *Nano Lett.* **2016**, 16, 7677.
- [42] W. Liu, Z. Chen, G. Zhou, Y. Sun, H. R. Lee, C. Liu, H. Yao, Z. Bao, Y. Cui, *Adv. Mater.* **2016**, 28, 3578.
- [43] S. Gong, W. Cheng, *Adv. Electron. Mater.* **2017**, 3, 1600314.
- [44] D. J. Lipomi, M. Vosgueritchian, B. C. Tee, S. L. Hellstrom, J. A. Lee, C. H. Fox, Z. Bao, *Nat. Nanotechnol.* **2011**, 6, 788.
- [45] T. Lv, Y. Yao, N. Li, T. Chen, *Angew. Chem. Int. Ed.* **2016**, 55, 9191.
- [46] Z. Zhang, J. Deng, X. Li, Z. Yang, S. He, X. Chen, G. Guan, J. Ren, H. Peng, *Adv. Mater.* **2015**, 27, 356.
- [47] P. Lee, J. Lee, H. Lee, J. Yeo, S. Hong, K. H. Nam, D. Lee, S. S. Lee, S. H. Ko, *Adv. Mater.* **2012**, 24, 3326.
- [48] a) Y. Tang, S. Gong, Y. Chen, L. W. Yap, W. Cheng, *ACS Nano* **2014**, 8, 5707; b) N. N. Jason, W. Shen, W. Cheng, *ACS Appl. Mater. Interfaces* **2015**, 7, 16760; c) N. N. Jason, S. J. Wang, S. Bhanushali, W. Cheng, *Nanoscale* **2016**, 8, 16596.
- [49] a) S. Gong, D. T. Lai, B. Su, K. J. Si, Z. Ma, L. W. Yap, P. Guo, W. Cheng, *Adv. Electron. Mater.* **2015**, 1, 1400063; b) S. Gong, D. T. Lai, Y. Wang, L. W. Yap, K. J. Si, Q. Shi, N. N. Jason, T. Sridhar, H. Uddin, W. Cheng, *ACS Appl. Mater. Interfaces* **2015**, 7, 19700.
- [50] a) S. Gong, Y. Zhao, L. W. Yap, Q. Shi, Y. Wang, J. A. P. Bay, D. T. Lai, H. Uddin, W. Cheng, *Adv. Electron. Mater.* **2016**, 2, 1600121; b) Y. Chen, Z. Ouyang, M. Gu, W. Cheng, *Adv. Mater.* **2013**, 25, 80.
- [51] S. Gong, Y. Zhao, Q. Shi, Y. Wang, L. W. Yap, W. Cheng, *Electroanalysis* **2016**, 28, 1298.
- [52] K. S. Kim, Y. Zhao, H. Jang, S. Y. Lee, J. M. Kim, K. S. Kim, J.-H. Ahn, P. Kim, J.-Y. Choi, B. H. Hong, *Nature* **2009**, 457, 706.
- [53] a) D. J. Lipomi, J. A. Lee, M. Vosgueritchian, B. C.-K. Tee, J. A. Bolander, Z. Bao, *Chem. Mater.* **2012**, 24, 373; b) D. J. Lipomi, B. C. K. Tee, M. Vosgueritchian, Z. Bao, *Adv. Mater.* **2011**, 23, 1771.
- [54] X. Zhang, Q. Li, Y. Tu, Y. Li, J. Y. Coulter, L. Zheng, Y. Zhao, Q. Jia, D. E. Peterson, Y. Zhu, *Small* **2007**, 3, 244.
- [55] J. Wang, X. Luo, T. Wu, Y. Chen, *Nat. Commun.* **2014**, 5, 3848.
- [56] W. Liu, M. S. Song, B. Kong, Y. Cui, *Adv. Mater.* **2016**, 29, 1603436.
- [57] C. Zhao, C. Wang, Z. Yue, K. Shu, G. G. Wallace, *ACS Appl. Mater. Interfaces* **2013**, 5, 9008.
- [58] Y. Wang, B. Li, J. Ji, A. Eyler, W. H. Zhong, *Adv. Energy Mater.* **2013**, 3, 1557.
- [59] a) H. Zhang, C. Liu, L. Zheng, W. Feng, Z. Zhou, J. Nie, *Electrochim. Acta* **2015**, 159, 93; b) D. P. Cole, A. L. M. Reddy, M. G. Hahn, R. McCotter, A. H. Hart, R. Vajtai, P. M. Ajayan, S. P. Karna, M. L. Bundy, *Adv. Energy Mater.* **2014**, 4, 1300844.
- [60] X. Wang, X. Lu, B. Liu, D. Chen, Y. Tong, G. Shen, *Adv. Mater.* **2014**, 26, 4763.
- [61] A. Yu, V. Chabot, J. Zhang, *Electrochemical Supercapacitors for Energy Storage and Delivery: Fundamentals and Applications*, first edition, CRC Press, Boca Raton, FL, **2013**.
- [62] Z. Yang, J. Deng, X. Chen, J. Ren, H. Peng, *Angew. Chem. Int. Ed.* **2013**, 52, 13453.
- [63] a) T. Chen, R. Hao, H. Peng, L. Dai, *Angew. Chem. Int. Ed.* **2015**, 54, 618; b) P. Xu, T. Gu, Z. Cao, B. Wei, J. Yu, F. Li, J. H. Byun, W. Lu, Q. Li, T. W. Chou, *Adv. Energy Mater.* **2014**, 4, 1300759.
- [64] Y. Xie, Y. Liu, Y. Zhao, Y. H. Tsang, S. P. Lau, H. Huang, Y. Chai, *J. Mater. Chem. A* **2014**, 2, 9142.
- [65] C. Choi, S. H. Kim, H. J. Sim, J. A. Lee, A. Y. Choi, Y. T. Kim, X. Lepró, G. M. Spinks, R. H. Baughman, S. J. Kim, *Sci. Rep.* **2015**, 5, 9387.
- [66] H. Wang, Z. Liu, J. Ding, X. Lepró, S. Fang, N. Jiang, N. Yuan, R. Wang, Q. Yin, W. Lv, Z. Liu, M. Zhang, R. Ovalle-Robles, K. Inoue, S. Yin, R. H. Baughman, *Adv. Mater.* **2016**, 28, 4998.
- [67] W. Ma, L. Song, R. Yang, T. Zhang, Y. Zhao, L. Sun, Y. Ren, D. Liu, L. Liu, J. Shen, Z. Zhang, Y. Xiang, W. Zhou, S. Xie, *Nano Lett.* **2007**, 7, 2307.
- [68] T. Gu, B. Wei, *J. Mater. Chem. A* **2016**, 4, 12289.
- [69] H. M. Jeong, J. W. Lee, W. H. Shin, Y. J. Choi, H. J. Chin, J. K. Kuang, J. W. Choi, *Nano Lett.* **2011**, 11, 2472.
- [70] X. Li, T. Gu, B. Wei, *Nano Lett.* **2012**, 12, 6366.
- [71] P. Xu, J. Kang, J.-B. Choi, J. Suhr, J. Yu, F. Li, J.-H. Byun, B.-S. Kim, T.-W. Chou, *ACS Nano* **2014**, 8, 9437.
- [72] T. Chen, H. Peng, M. Durstock, L. Dai, *Sci. Rep.* **2014**, 4, 3612.
- [73] D. Kim, G. Shin, Y. J. Kang, W. Kim, J. S. Ha, *ACS Nano* **2013**, 7, 7975.

- [74] D. Kim, J. Yun, G. Lee, J. S. Ha, *Nanoscale* **2014**, 6, 12034.
- [75] U. Gulzar, S. Goriparti, E. Miele, T. Li, G. Maidecchi, A. Toma, F. De Angelis, C. Capiglia, R. P. Zaccaria, *J. Mater. Chem. A* **2016**, 4, 16771.
- [76] Y.-H. Lee, Y. Kim, T.-I. Lee, I. Lee, J. Shin, H. S. Lee, T.-S. Kim, J. W. Choi, *ACS Nano* **2015**, 9, 12214.
- [77] F. X. Ma, H. Hu, H. B. Wu, C. Y. Xu, Z. Xu, L. Zhen, *Adv. Mater.* **2015**, 27, 4097.
- [78] Z. Niu, W. Zhou, X. Chen, J. Chen, S. Xie, *Adv. Mater.* **2015**, 27, 6002.
- [79] L. Wen, F. Li, H. M. Cheng, *Adv. Mater.* **2016**, 28, 4306.
- [80] M. Koo, K.-I. Park, S. H. Lee, M. Suh, D. Y. Jeon, J. W. Choi, K. Kang, K. J. Lee, *Nano Lett.* **2012**, 12, 4810.
- [81] H. Lin, W. Weng, J. Ren, L. Qiu, Z. Zhang, P. Chen, X. Chen, J. Deng, Y. Wang, H. Peng, *Adv. Mater.* **2014**, 26, 1217.
- [82] Y. Zhang, W. Bai, J. Ren, W. Weng, H. Lin, Z. Zhang, H. Peng, *J. Mater. Chem. A* **2014**, 2, 11054.
- [83] J. Ren, Y. Zhang, W. Bai, X. Chen, Z. Zhang, X. Fang, W. Weng, Y. Wang, H. Peng, *Angew. Chem.* **2014**, 126, 7998.
- [84] Y. Zhang, W. Bai, X. Cheng, J. Ren, W. Weng, P. Chen, X. Fang, Z. Zhang, H. Peng, *Angew. Chem.* **2014**, 126, 14792.
- [85] Y. Zhang, C. J. Sheehan, J. Zhai, G. Zou, H. Luo, J. Xiong, Y. Zhu, Q. Jia, *Adv. Mater.* **2010**, 22, 3027.
- [86] H. Lee, J. K. Yoo, J. H. Park, J. H. Kim, K. Kang, Y. S. Jung, *Adv. Energy Mater.* **2012**, 2, 976.
- [87] G. H. Lee, J. W. Lee, J. I. Choi, S. J. Kim, Y.-H. Kim, J. K. Kang, *Adv. Funct. Mater.* **2016**, 26, 5139.
- [88] W. Weng, Q. Sun, Y. Zhang, S. He, Q. Wu, J. Deng, X. Fang, G. Guan, J. Ren, H. Peng, *Adv. Mater.* **2015**, 27, 1363.
- [89] a) J. Chen, F. Cheng, *Acc. Chem. Res.* **2009**, 42, 713; b) P. Hiralal, S. Imaizumi, H. E. Unalan, H. Matsumoto, M. Minagawa, M. Rouvala, A. Tanioka, G. A. Amaratunga, *ACS Nano* **2010**, 4, 2730; c) A. M. Gaikwad, A. M. Zamarayeva, J. Rousseau, H. Chu, I. Derin, D. A. Steingart, *Adv. Mater.* **2012**, 24, 5071.
- [90] M. Kaltenbrunner, G. Kettlgruber, C. Siket, R. Schwödauer, S. Bauer, *Adv. Mater.* **2010**, 22, 2065.
- [91] R. Pelrine, R. Kornbluh, Q. Pei, J. Joseph, *Science* **2000**, 287, 836.
- [92] C. Yan, X. Wang, M. Cui, J. Wang, W. Kang, C. Y. Foo, P. S. Lee, *Adv. Energy Mater.* **2014**, 4, 1301396.
- [93] K. T. Braam, S. K. Volkman, V. Subramanian, *J. Power Sources* **2012**, 199, 367.
- [94] R. Kumar, J. Shin, L. Yin, J. You, Y. S. Meng, J. Wang, *Adv. Energy Mater.* **2016**, 6, 1602096.
- [95] Y. Xu, Y. Zhang, Z. Guo, J. Ren, Y. Wang, H. Peng, *Angew. Chem. Int. Ed.* **2015**, 54, 15390.
- [96] Y. Xu, Y. Zhao, J. Ren, Y. Zhang, H. Peng, *Angew. Chem.* **2016**, 128, 8111.
- [97] a) N. L. Panwar, S. C. Kaushik, S. Kothari, *Renew. Sustainable Energy Rev.* **2011**, 15, 1513; b) M. Tao, *Electrochem. Soc. Interface* **2008**, 17, 30.
- [98] S. B. Darling, F. You, *RSC Adv.* **2013**, 3, 17633.
- [99] R. W. Miles, G. Zoppi, I. Forbes, *Mater. Today* **2007**, 10, 20.
- [100] J. Lee, J. Wu, M. Shi, J. Yoon, S. I. Park, M. Li, Z. Liu, Y. Huang, J. A. Rogers, *Adv. Mater.* **2011**, 23, 986.
- [101] J. Lee, J. Wu, J. H. Ryu, Z. Liu, M. Meitl, Y. W. Zhang, Y. Huang, J. A. Rogers, *Small* **2012**, 8, 1851.
- [102] J. Nam, Y. Lee, W. Choi, C. S. Kim, H. Kim, J. Kim, D.-H. Kim, S. Jo, *Adv. Energy Mater.* **2016**, 6, 1601269.
- [103] G. Li, R. Zhu, Y. Yang, *Nat. Photon.* **2012**, 6, 153.
- [104] M. Kaltenbrunner, M. S. White, E. D. Głowacki, T. Sekitani, T. Someya, N. S. Sariciftci, S. Bauer, *Nat. Commun.* **2012**, 3, 770.
- [105] T. Kim, J.-H. Kim, T. E. Kang, C. Lee, H. Kang, M. Shin, C. Wang, B. Ma, U. Jeong, T.-S. Kim, B. J. Kim, *Nat. Commun.* **2015**, 6, 8547.
- [106] T. F. O'Connor, A. V. Zaretski, B. A. Shiravi, S. Savagatrup, A. D. Printz, M. I. Diaz, D. J. Lipomi, *Energy Environ. Sci.* **2014**, 7, 370.
- [107] S. Savagatrup, A. D. Printz, H. Wu, K. M. Rajan, E. J. Sawyer, A. V. Zaretski, C. J. Bettinger, D. J. Lipomi, *Synth. Met.* **2015**, 203, 208.
- [108] T. F. O'Connor, A. V. Zaretski, S. Savagatrup, A. D. Printz, C. D. Wilkes, M. I. Diaz, E. J. Sawyer, D. J. Lipomi, *Sol. Energ. Mat. Sol. Cells* **2016**, 144, 438.
- [109] Z. Yang, J. Deng, X. Sun, H. Li, H. Peng, *Adv. Mater.* **2014**, 26, 2643.
- [110] a) T. Chen, L. Qiu, H. Li, H. Peng, *J. Mater. Chem.* **2012**, 22, 23655; b) R. Li, X. Xiang, X. Tong, J. Zou, Q. Li, *Adv. Mater.* **2015**, 27, 3831.
- [111] L. Qiu, J. Deng, X. Lu, Z. Yang, H. Peng, *Angew. Chem. Int. Ed.* **2014**, 53, 10425.
- [112] D.-Y. Cho, K. Eun, S.-H. Choa, H.-K. Kim, *Carbon* **2014**, 66, 530.
- [113] N. Zhang, J. Chen, Y. Huang, W. Guo, J. Yang, J. Du, X. Fan, C. Tao, *Adv. Mater.* **2016**, 28, 263.
- [114] C.-Y. Sue, N.-C. Tsai, *Appl. Energy* **2012**, 93, 390.
- [115] a) J. Yun, S. N. Patel, M. S. Reynolds, G. D. Abowd, *IEEE Trans. Mob. Comput.* **2011**, 10, 669; b) G. T. Hwang, H. Park, J. H. Lee, S. Oh, K. I. Park, M. Byun, H. Park, G. Ahn, C. K. Jeong, K. No, H. Kwon, S. Lee, B. Joung, K. J. Lee, *Adv. Mater.* **2014**, 26, 4880; c) Y. Qi, M. C. McAlpine, *Energy Environ. Sci.* **2010**, 3, 1275; d) M. Lee, C. Y. Chen, S. Wang, S. N. Cha, Y. J. Park, J. M. Kim, L. J. Chou, Z. L. Wang, *Adv. Mater.* **2012**, 24, 1759.
- [116] Z. Li, G. Zhu, R. Yang, A. C. Wang, Z. L. Wang, *Adv. Mater.* **2010**, 22, 2534.
- [117] M. Deterre, E. Lefevre, Y. Zhu, M. Woytasik, B. Boutaud, R. Dal Molin, *J. Microelectromech. Syst.* **2014**, 23, 651.
- [118] R. Riemer, A. Shapiro, *J. Neuroeng. Rehabil.* **2011**, 8, 22.
- [119] C. Sun, J. Shi, D. J. Bayerl, X. Wang, *Energy Environ. Sci.* **2011**, 4, 4508.
- [120] R. Yang, Y. Qin, C. Li, G. Zhu, Z. L. Wang, *Nano Lett.* **2009**, 9, 1201.
- [121] L. Persano, C. Dagdeviren, Y. Su, Y. Zhang, S. Girardo, D. Pisignano, Y. Huang, J. A. Rogers, *Nat. Commun.* **2013**, 4, 1633.
- [122] Y. Qi, J. Kim, T. D. Nguyen, B. Lisko, P. K. Purohit, M. C. McAlpine, *Nano Lett.* **2011**, 11, 1331.
- [123] H. Kim, Y. Tadesse, S. Priya, in *Energy Harvesting Technologies*, (Eds: S. Priya, D. J. Inman), first edition, Springer, New York, NY, **2009**.
- [124] T. Starner, *IBM Syst. J.* **1996**, 35, 618.
- [125] O. Guillon, F. Thiebaud, D. Perreux, *Int. J. Fract.* **2002**, 117, 235.
- [126] J. Chun, N.-R. Kang, J.-Y. Kim, M.-S. Noh, C.-Y. Kang, D. Choi, S.-W. Kim, Z. L. Wang, J. M. Baik, *Nano Energy* **2015**, 11, 1.
- [127] a) Y. Huang, N. Bu, Y. Duan, Y. Pan, H. Liu, Z. Yin, Y. Xiong, *Nanoscale* **2013**, 5, 12007; b) Y. Duan, Y. Huang, Z. Yin, N. Bu, W. Dong, *Nanoscale* **2014**, 6, 3289.
- [128] C. K. Jeong, J. Lee, S. Han, J. Ryu, G. T. Hwang, D. Y. Park, J. H. Park, S. S. Lee, M. Byun, S. H. Ko, *Adv. Mater.* **2015**, 27, 2866.
- [129] F.-R. Fan, Z.-Q. Tian, Z. L. Wang, *Nano Energy* **2012**, 1, 328.
- [130] Z. L. Wang, *Mater. Today* **2017**, 20, 74.
- [131] S. Park, H. Kim, M. Vosgueritchian, S. Cheon, H. Kim, J. H. Koo, T. R. Kim, S. Lee, G. Schwartz, H. Chang, Z. Bao, *Adv. Mater.* **2014**, 26, 7324.
- [132] B.-U. Hwang, J.-H. Lee, T. Q. Trung, E. Roh, D.-I. Kim, S.-W. Kim, N.-E. Lee, *ACS Nano* **2015**, 9, 8801.
- [133] F. Yi, L. Lin, S. Niu, P. K. Yang, Z. Wang, J. Chen, Y. Zhou, Y. Zi, J. Wang, Q. Liao, Y. Zhang, Z. L. Wang, *Adv. Funct. Mater.* **2015**, 25, 3688.
- [134] P. K. Yang, L. Lin, F. Yi, X. Li, K. C. Pradel, Y. Zi, C. I. Wu, H. He Jr., Y. Zhang, Z. L. Wang, *Adv. Mater.* **2015**, 27, 3817.
- [135] K. N. Kim, J. Chun, J. W. Kim, K. Y. Lee, J.-U. Park, S.-W. Kim, Z. L. Wang, J. M. Baik, *ACS Nano* **2015**, 9, 6394.
- [136] J. H. We, S. J. Kim, B. J. Cho, *Energy* **2014**, 73, 506.
- [137] S. J. Kim, J. H. We, B. J. Cho, *Energy Environ. Sci.* **2014**, 7, 1959.

- [138] J. Reeder, M. Kaltenbrunner, T. Ware, D. Arreaga-Salas, A. Avendano-Bolivar, T. Yokota, Y. Inoue, M. Sekino, W. Voit, T. Sekitani, T. Someya, *Adv. Mater.* **2014**, *26*, 4967.
- [139] P. Luan, N. Zhang, W. Zhou, Z. Niu, Q. Zhang, L. Cai, X. Zhang, F. Yang, Q. Fan, W. Zhou, Z. Xiao, Xiao Gu, H. Chen, K. Li, S. Xiao, Y. Wang, H. Liu, S. Xie, *Adv. Funct. Mater.* **2016**, *26*, 8178.
- [140] C. Pang, J. H. Koo, A. Nguyen, J. M. Caves, M. G. Kim, A. Chortos, K. Kim, P. J. Wang, J. B. H. Tok, Z. Bao, *Adv. Mater.* **2015**, *27*, 634.
- [141] S. Wang, M. Li, J. Wu, D.-H. Kim, N. Lu, Y. Su, Z. Kang, Y. Huang, J. A. Rogers, *J. Appl. Mech.* **2012**, *79*, 031022.
- [142] W. H. Yeo, Y. S. Kim, J. Lee, A. Ameen, L. Shi, M. Li, S. Wang, R. Ma, S. H. Jin, Z. Kang, Y. Huang, J. A. Rogers, *Adv. Mater.* **2013**, *25*, 2773.
- [143] C. Pang, J. H. Koo, A. Nguyen, J. M. Caves, M.-G. Kim, A. Chortos, K. Kim, P. J. Wang, J. B.-H. Tok, Z. Bao, *Adv. Mater.* **2015**, *27*, 634.
- [144] H. Wang, B. Zhu, W. Jiang, Y. Yang, W. R. Leow, H. Wang, X. Chen, *Adv. Mater.* **2014**, *26*, 3638.
- [145] L. Yin, X. Huang, H. Xu, Y. Zhang, J. Lam, J. Cheng, J. A. Rogers, *Adv. Mater.* **2014**, *26*, 3879.
- [146] J. W. Lee, R. Xu, S. Lee, K.-I Jang, Y. Yang, A. Banks, K. J. Yu, J. Kim, S. Xu, S. Ma, S. W. Jang, P. Won, Y. Li, B. H. Kim, J. Y. Choe, S. Huh, Y. H. Kwon, Y. Huang, U. Paik, J. A. Rogers, *Proc. Natl. Acad. Sci. U.S.A.* **2016**, *113*, 6131.
- [147] Y.-H. Lee, J.-S. Kim, J. Noh, I. Lee, H. J. Kim, S. Choi, J. Seo, S. Jeon, T.-S. Kim, J.-Y. Lee, J. W. Choi, *Nano Lett.* **2013**, *13*, 5753.
- [148] S. Jung, S. Hong, J. Kim, S. Lee, T. Hyeon, M. Lee, D.-H. Kim, *Sci. Rep.* **2015**, *5*, 17081.
- [149] J. Wang, S. Li, F. Yi, Y. Zi, J. Lin, X. Wang, Y. Xu, Z. L. Wang, *Nat. Commun.* **2016**, *7*, 12744.
- [150] Z. Wen, M.-H. Yeh, H. Guo, J. Wang, Y. Zi, W. Xu, J. Deng, L. Zhu, X. Wang, C. Hu, L. Zhu, X. Sun, Z. L. Wang, *Sci. Adv.* **2016**, *2*, e1600097.
- [151] K. Song, J. H. Han, T. Lim, N. Kim, S. Shin, J. Kim, H. Choo, S. Jeong, Y.-C. Kim, Z. L. Wang, J. Lee, *Adv. Healthcare Mater.* **2016**, *5*, 1572.
- [152] Q. Zheng, Y. Zou, Y. Zhang, Z. Liu, B. Shi, X. Wang, Y. Jin, H. Ouyang, Z. Li, Z. L. Wang, *Sci. Adv.* **2016**, *2*, e1501478.
- [153] E. Katz, K. MacVittie, *Energy Environ. Sci.* **2013**, *6*, 2791.
- [154] A. J. Bandodkar, I. Jeerapan, J.-M. You, R. Nuñez-Flores, J. Wang, *Nano Lett.* **2016**, *16*, 721.
- [155] A. Haeblerlin, A. Zurbuchen, J. Schaerer, J. Wagner, S. Walpen, C. Huber, H. Haeblerlin, J. Fuhrer, R. Vogel, *Europace* **2014**, *16*, 1534.
- [156] A. Haeblerlin, A. Zurbuchen, S. Walpen, J. Schaerer, T. Niederhauser, C. Huber, H. Tanner, H. Servatius, J. Seiler, H. Haeblerli, J. Fuhrer, R. Vogel, *Heart Rhythm* **2015**, *12*, 1317.
- [157] S.-W. Hwang, H. Tao, D.-H. Kim, H. Cheng, J.-K. Song, E. Rill, M. A. Brenckle, B. Panilaitis, S. M. Won, Y.-S. Kim, Y. M. Song, K. J. Yu, A. Ameen, R. Li, Y. Su, M. Yang, D. L. Kaplan, M. R. Zakin, M. J. Slepian, Y. Huang, F. G. Omenetto, J. A. Rogers, *Science* **2012**, *337*, 1640.
- [158] C. Dagdeviren, S.-W. Hwang, Y. Su, S. Kim, H. Cheng, O. Gur, R. Haney, F. G. Omenetto, Y. Huang, J. A. Rogers, *Small* **2013**, *9*, 3398.
- [159] S.-W. Hwang, C. H. Lee, H. Cheng, J.-W. Jeong, S.-K. Kang, J.-H. Kim, J. Shin, J. Yang, Z. Liu, G. A. Ameer, Y. Huang, J. A. Rogers, *Nano Lett.* **2015**, *15*, 2801.
- [160] J. Kim, P. Gutruf, A. M. Chiarelli, S. Y. Heo, K. Cho, Z. Xie, A. Banks, S. Han, K. I. Jang, J. W. Lee, K.-T. Lee, X. Feng, Y. Huang, M. Fabiani, G. Gratton, U. Paik, J. A. Rogers, *Adv. Funct. Mater.* **2017**, *27*, 1604373.
- [161] K. Y. Lee, H. J. Yoon, T. Jiang, X. Wen, W. Seung, S. W. Kim, Z. L. Wang, *Adv. Energy Mater.* **2016**, *6*, 1502566.